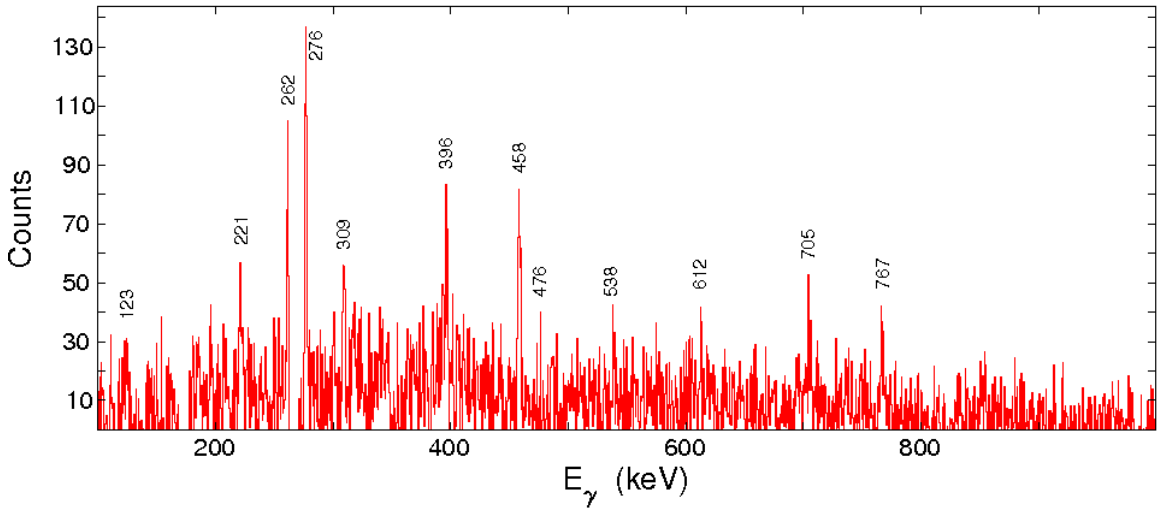

Fig 4-6 gate 492 keV transition

Gating on the gamma ray below 458 keV transition, i.e. 309 keV peak, one notices another interesting feature that the spectra gated on 315 keV, 458 keV and 492 keV transitions do not have (see Fig. 4-7). These are the p keV. This shows that the 773 keV and 950 keV transitions a)9 keV peak but in anti-coincidence with 458 keV, 315 ke s. Furthermore the sums 315 keV+458 keV and 458 keV+4 to 773 keV and 950 keV respectively.

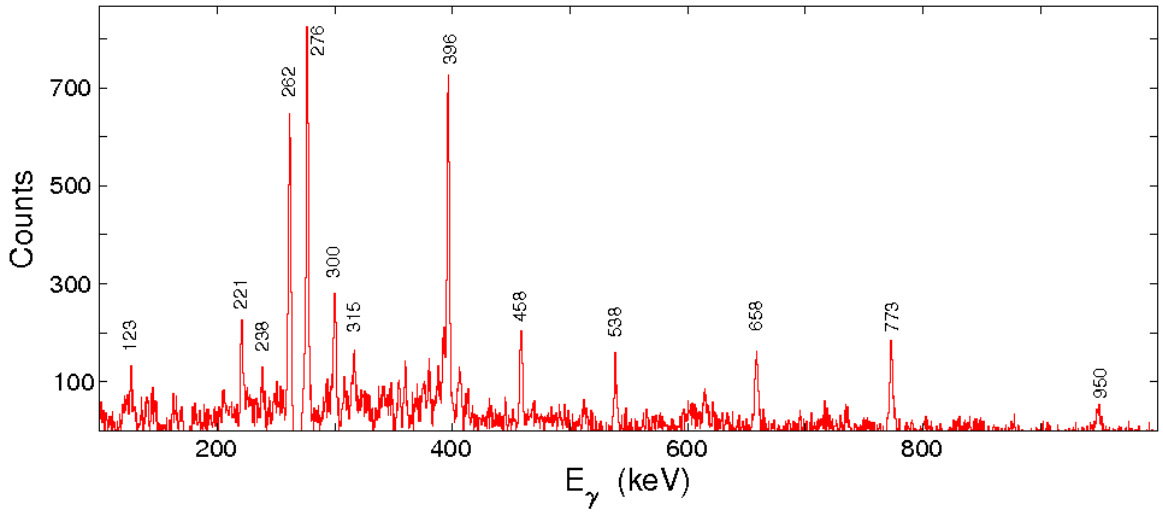

Fig 4-7 gate on 309 keV transition

This suggests that the 773 keV and 950 keV peaks can be cross-overs to the 315 keV and 458 keV peaks, and to 492 keV and 458 keV transitions respectively. This is further confirmed by gating on 773 keV and 950 keV transitions. The 773 keV gated spectrum

confirms that 773 keV transition is in anti-coincidence with 315 keV and 458 keV transitions (by their absence) and in coincidence with the other transitions in band1 (see Fig 4-8). Similarly gating on 950 keV transition confirms the anti-coincidence of 950 keV peak with the 492 keV and 458 keV peaks while 950 keV transition remains in coincidence with the other transitions of band1 (see Fig 4-8).Thus the placement in band 1 of these new transitions is established. It is shown in Fig. 4-14.

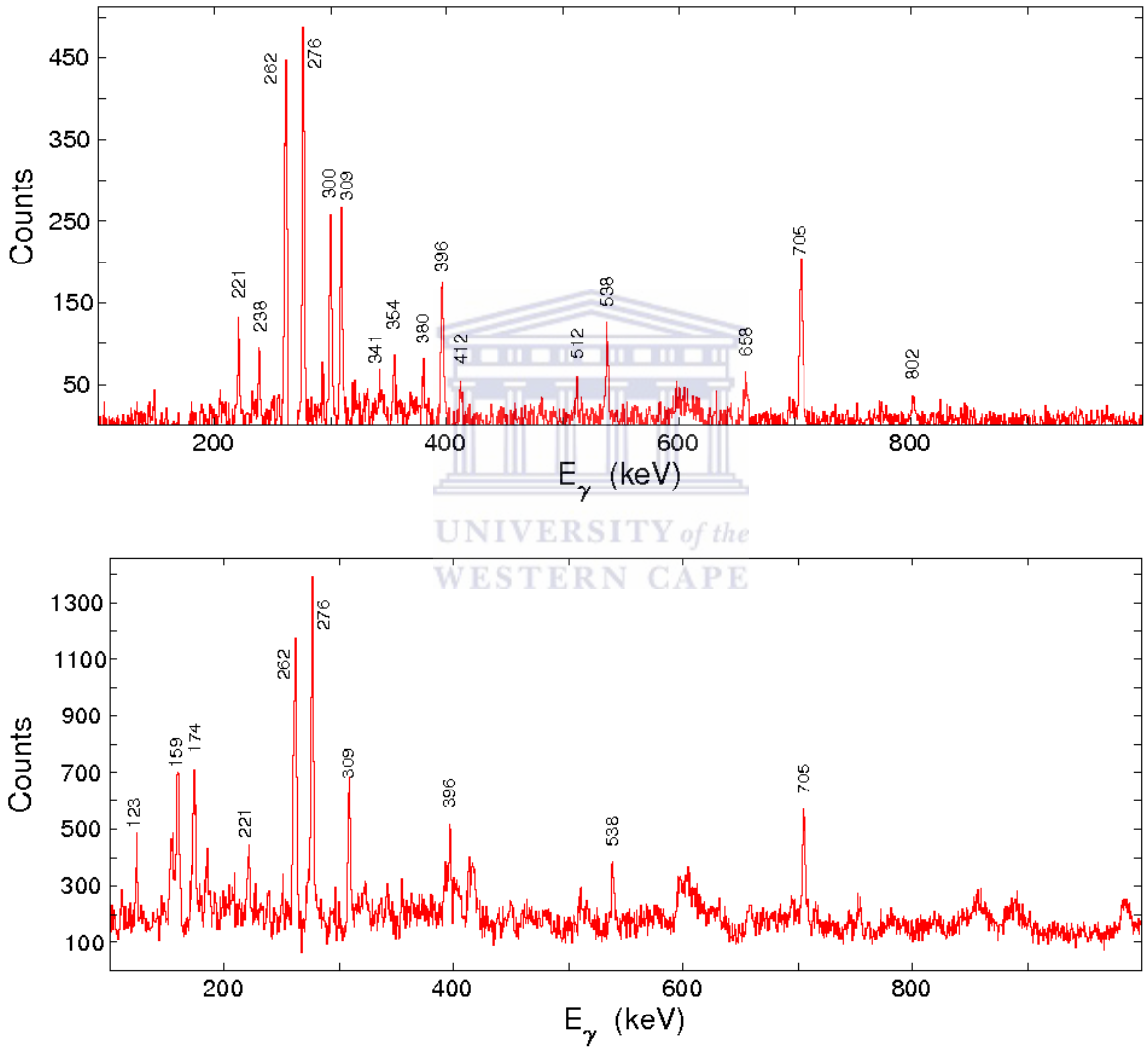

Fig 4-8 gates on 773 keV (top) and 950 keV (bottom) peaks

Gating on 315 keV transition (see Fig. 4-5), we see that 300 keV peak is equally strong as 458 keV peak suggesting that 300 keV peak may be placed directly above 315 keV transition. To confirm such a placement a cross-over transition is needed. The cross-over would be seen in the spectrum gated on 458 keV transition but would disappear in the spectra gated on

transitions 300 keV, or 773 keV, or 315 keV, or 492 keV, or 950 keV. The peak 615 keV is indeed observed in the spectrum gated on peak 458 keV (see Fig 4-3) while it is not seen in the spectra gated on peaks 300 keV, 773 keV, 315 keV, 492 keV and 950 keV. The cross-over is expected to have energy of 315 keV+ 300 keV=615 keV. The spectrum gated on 615 keV peak, Fig. 4-9 further confirms the placement of 615 keV as a cross-over of 315 keV and 300 keV transitions.

There could be a transition linking the levels at the excitation energy of 2669 MeV and 2546 MeV. If so its energy will be 615 keV-492 keV= 123 keV. In Fig. 4-7 which shows a spectrum gated on 309 keV peak, a transition with energy 123 keV is observed. Furthermore the spectrum gated on 123 keV transition (see Fig. 4-10) shows a coincidence with the other transitions in band1, including 492 keV and 950 keV gamma rays, but not with 615 keV and 300 keV gamma rays. Thus the 123keV transition was placed above the 492 keV transition in anti-coincidence with the 615keV transition.

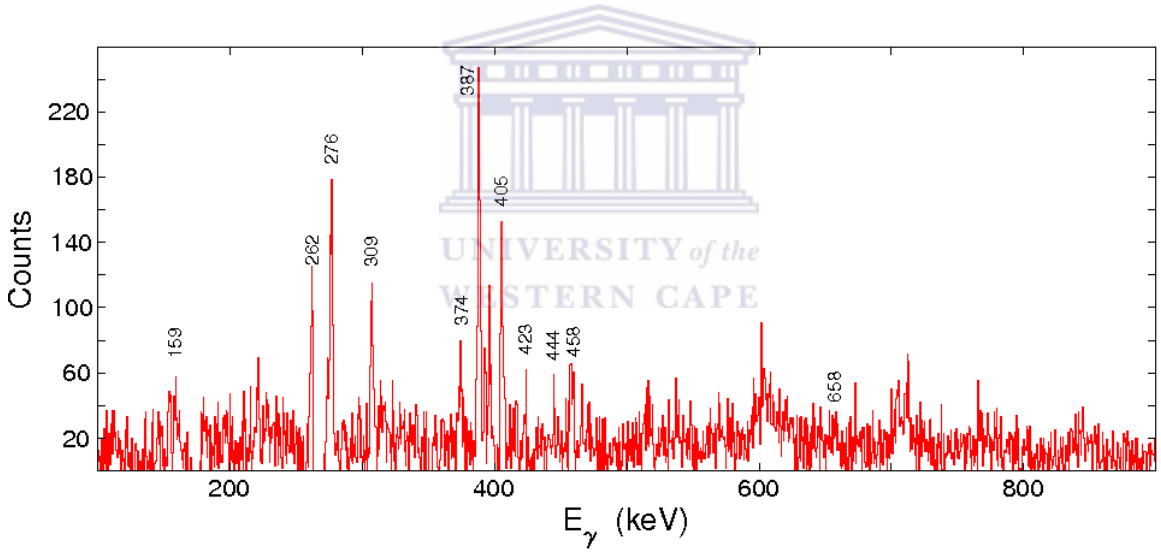

Fig 4-9 Gate on 615 keV transition

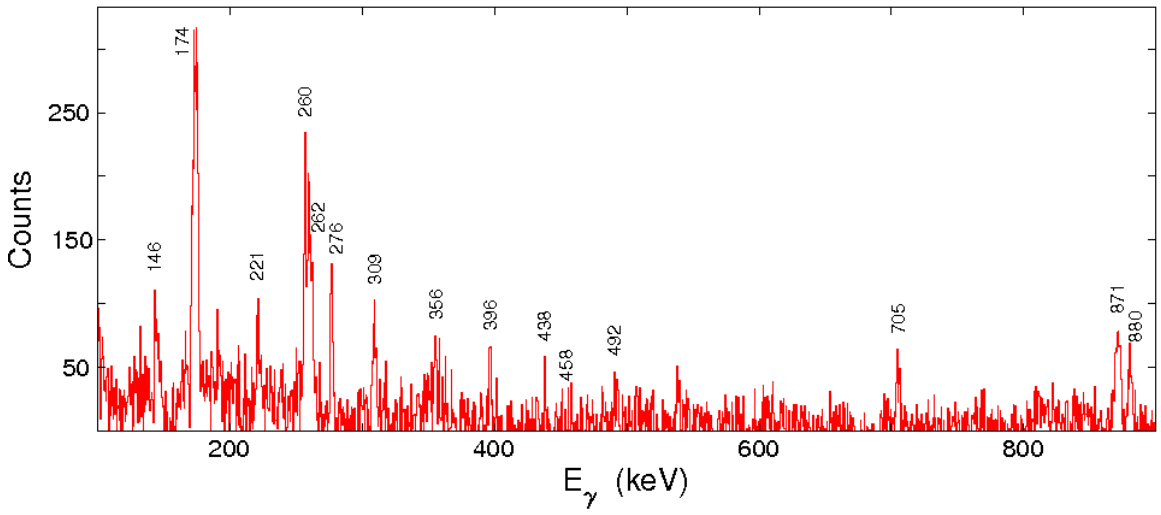

Fig 4-10 gate on 123 keV transition

In the spectrum gated on 300 keV (see Fig. 4-11) one notices a strong, still to be placed, peak, i.e. 221 keV. Furthermore a closer look at 262 keV (see Fig. 4-11) shows that the peak is very broad thus suggesting that another peak is located at a very close energy to 262 keV. In the gate on 221 keV spectrum (see Fig. 4-12), a very strong peak with energy closer to 260 keV is seen. Further gating proved that both of the transitions, 260 keV and 221 keV are in coincidence with the gamma rays of band1 and with each other and should thus be placed above the 300 keV transition. Since no cross-over transition could be found at this time the ordering of these two transitions is not unambiguous.

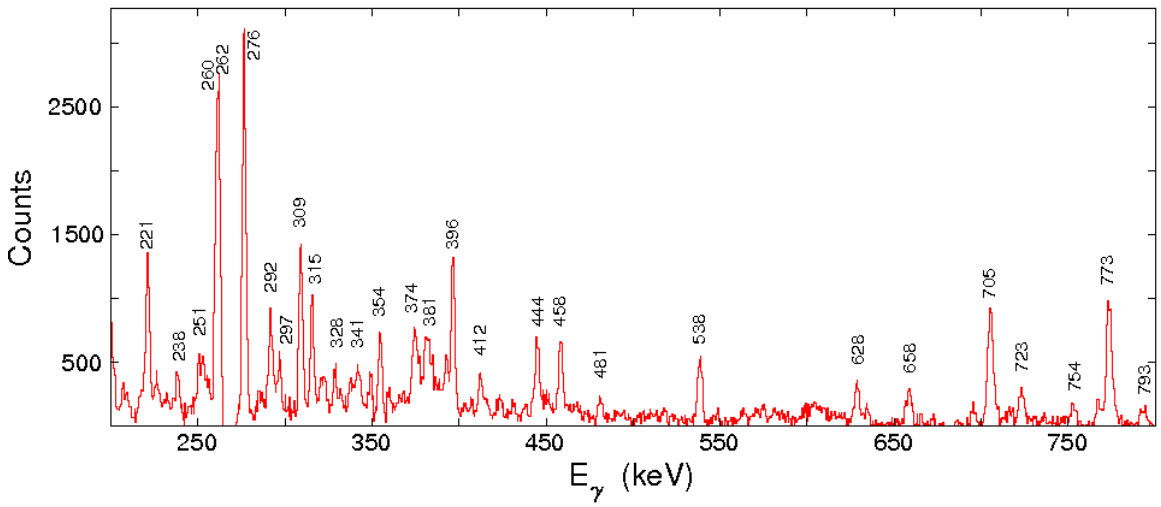

Fig 4-11 Gate on 300 keV transition

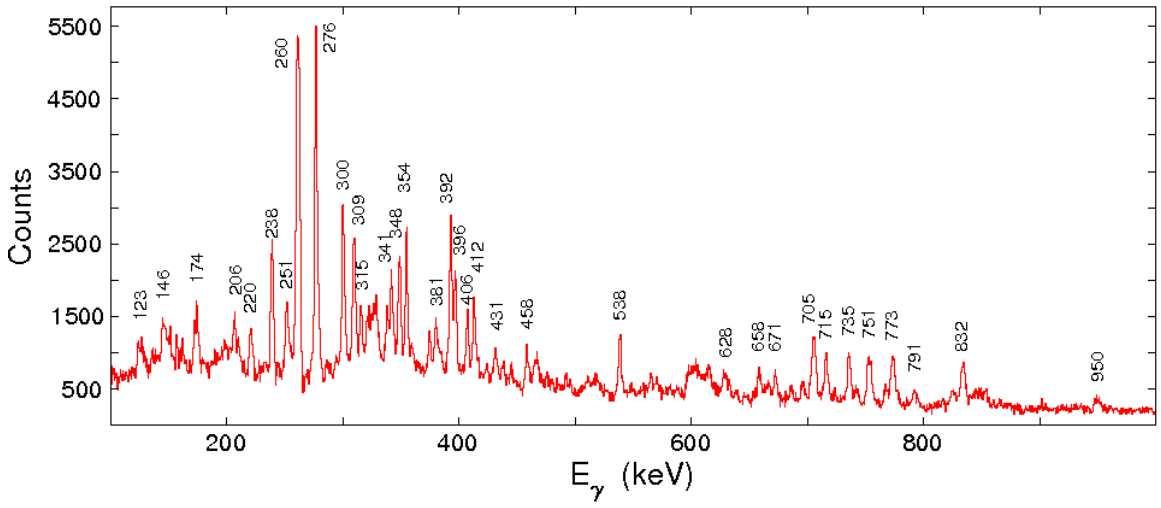

Fig 4-12 Gate on 221 keV transition

Similarly the transitions 354 kev, 341 keV and 412 keV were placed above the 221 keV gamma ray in the level scheme (see Fig. 4-14). Since no cross-overs were found, the ordering of these gamma rays could be different. Another transition, 238 keV is found in anti-coincidence with 354 keV, 341 keV and 412 keV peaks (see Fig. 4-13), which explains the placement shown in Fig. 4-14.

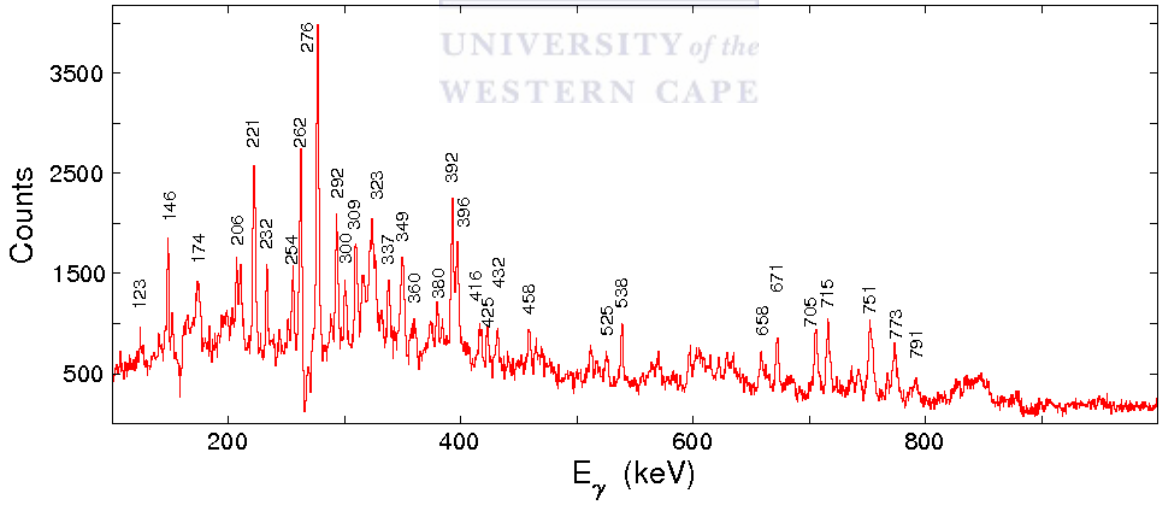

fig 4-13 Gate 238 keV transition

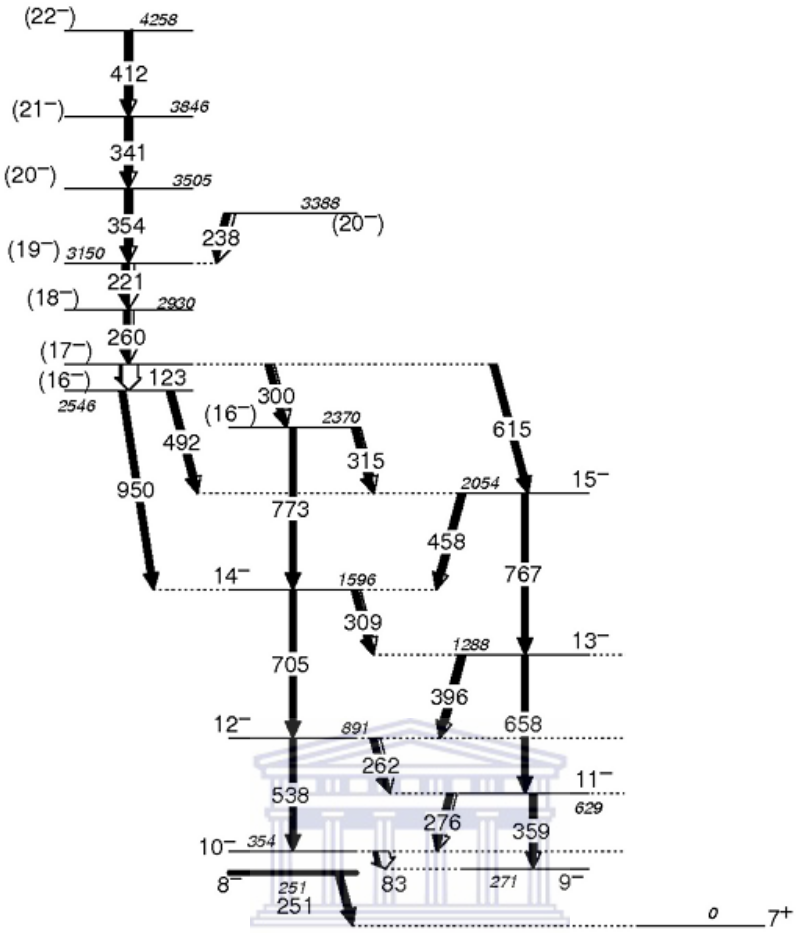

Fig 4-14 Yrast band1, known band plus new transitions

4.2.1.3 **Band2**

Looking at the total projection as shown in Fig. 4-1, the peak 297 keV is quite dominant and not yet placed in the level scheme. Gating on 297 keV transition (see Fig. 4-15) one sees a few interesting features.

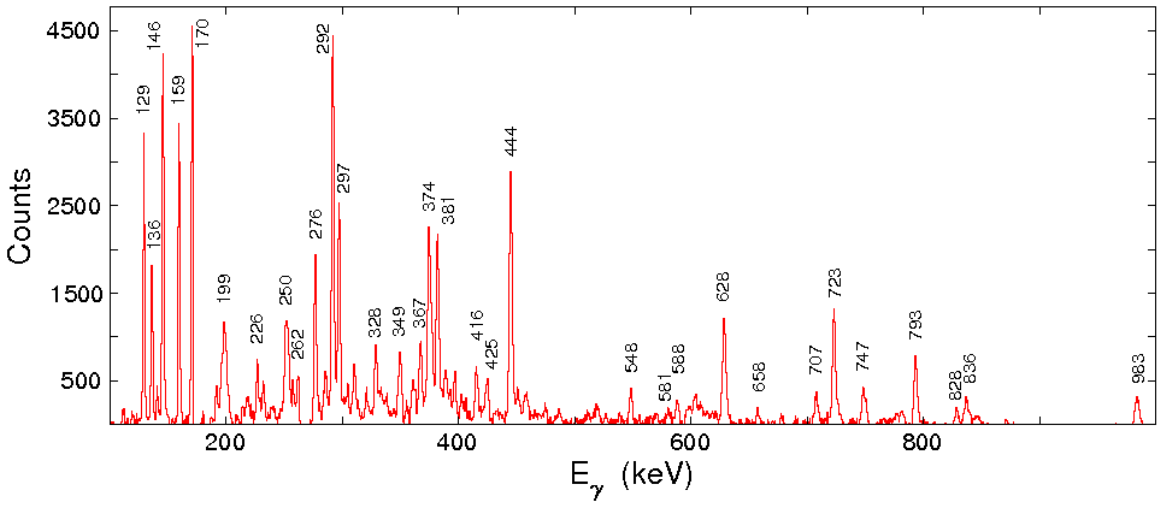

Fig 4-15 Gate on 297 keV transition

The first thing one notices is the several new and very intense gamma rays with energies of 292 keV, 170 keV and 146 keV. The second thing one notices is that the peak 297 keV is a doublet. Doublets are tricky to place. 297 keV transition is a doublet since a peak at 297 keV appears in the spectrum gated on the 297 keV transition. Thus one 297 keV transition has to be in coincidence with another 297 keV transition. Further analysis of the coincidences shows that the strong peaks at 297 keV, 146 keV, 159 keV, 170 keV and 292 keV are all in coincidence with each other, thus they have to belong in one decay path. Fig 4-15 shows two out of several possible placements. When examining the intensity of 297 keV transition as seen from the spectrum gated of 297 keV peak, as in Fig. 4-15, one would think that the 297 keV transitions should not be placed on top of each other but rather further away from each other, since the peak 297 keV is not very strong. Another important feature observed in this gated spectrum is the absence of transitions from band1 placed above the 396 keV gamma-ray.

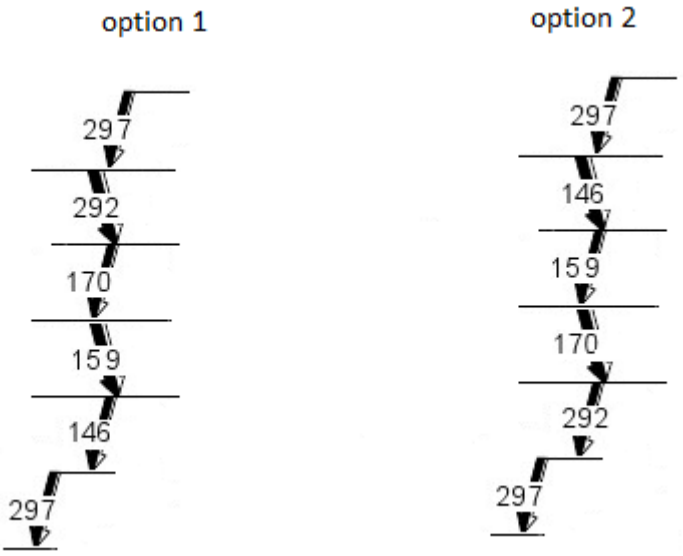

Fig 4-16 Two possible placements of the six transitions which belong to one decay path

Thus the 297 keV transition should in some way be linked to the lower part of band1. The third important feature in this gated spectrum is the presence of strong high energy gamma rays. These include the transition 445 keV, 628 keV, 707 keV, 723 keV, 747 keV, 793 keV, 836 keV and 983 keV. The high energy transitions have two important roles in a level scheme. The first role is that they can be potential cross-overs and the second role they play is that they may link different bands. Investigation of these high energy gamma rays could potentially link the new structure to band1. Starting with the highest energy gamma ray we examined them. The spectrum gated on 983 keV transition is shown in Fig. 4-17.

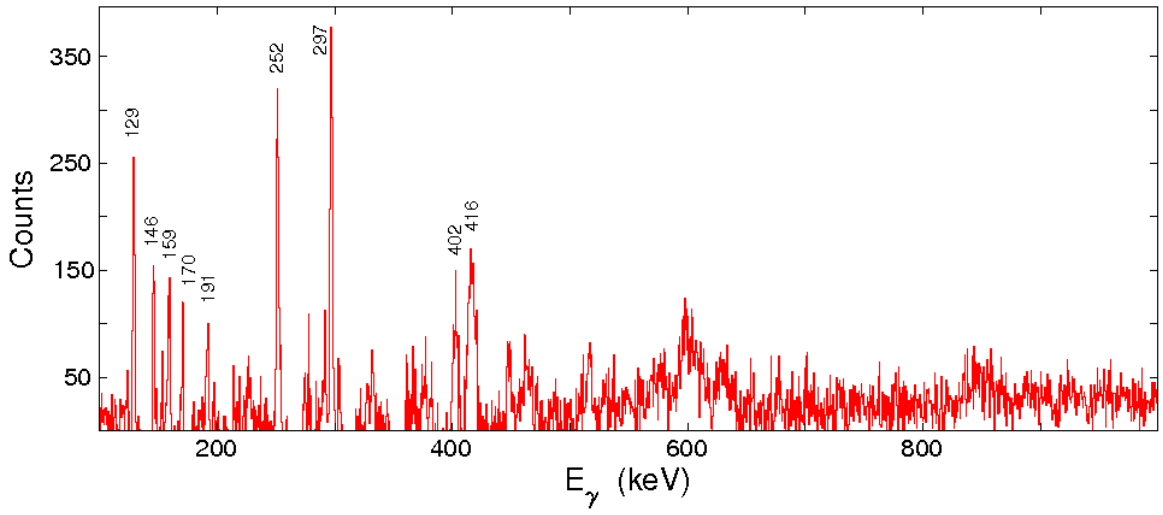

Fig 4-17 Gate on 983 keV transition

This spectrum shows strong 297 keV, 252 keV and 129 keV peaks. The gate on 983 keV transition does not present any evidence yet for the placement of 983 keV peak, except that it is in coincidence with the transitions of the new structure (as shown in Fig. 4-16).

Gating on 836 keV transition, which was the next highest energy gamma ray we see the spectrum shown in Fig. 4-18

There are two strong peaks at 276 keV and 297 keV, while the peak at 129 keV disappears. This shows that 129 keV transition is in coincidence with 983 keV and 297 keV peaks (see Fig. 4-17), while 836 keV transition is in coincidence with 276 keV and 297 keV peaks but anti-coincidence with 129 keV gamma-ray (see Fig. 4-18). One can also notice that 983 keV+129 keV= 276 keV+836 keV. Further analysis of the gated spectra convinced us to place 836 keV transition directly on top of the 11^- level of band1 and 983keV transition on top of the 10^- level of band1 with 129 keV transition in anti-coincidence with 836 keV peak, as shown in Fig. 4-19.

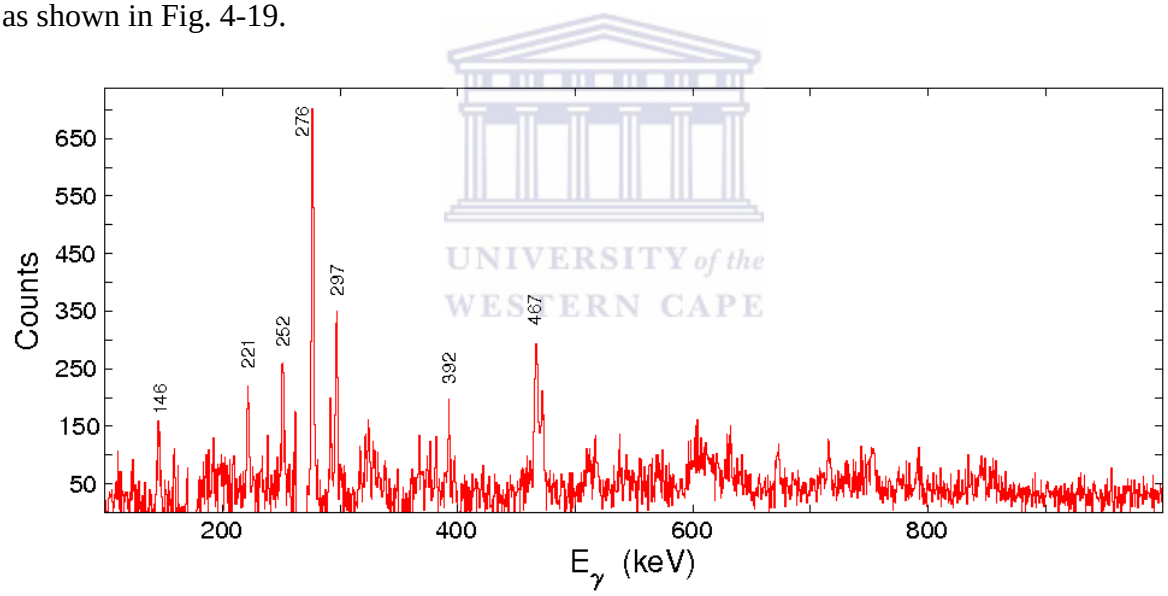

Fig 4-18 Gate on 836 keV transition

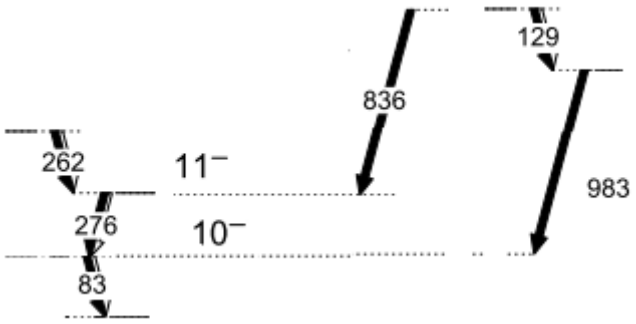

Fig 4-19 The placement of 129 keV, 836 keV and 983 keV transitions.

The next step was to figure out how to place the remaining strong transitions, i.e. 297 keV, 146 keV, 159 keV, 170 keV, 292 keV transitions, etc. Gating on 145 keV transition (see Fig. 4-20) we see the 297 keV peak very strongly.

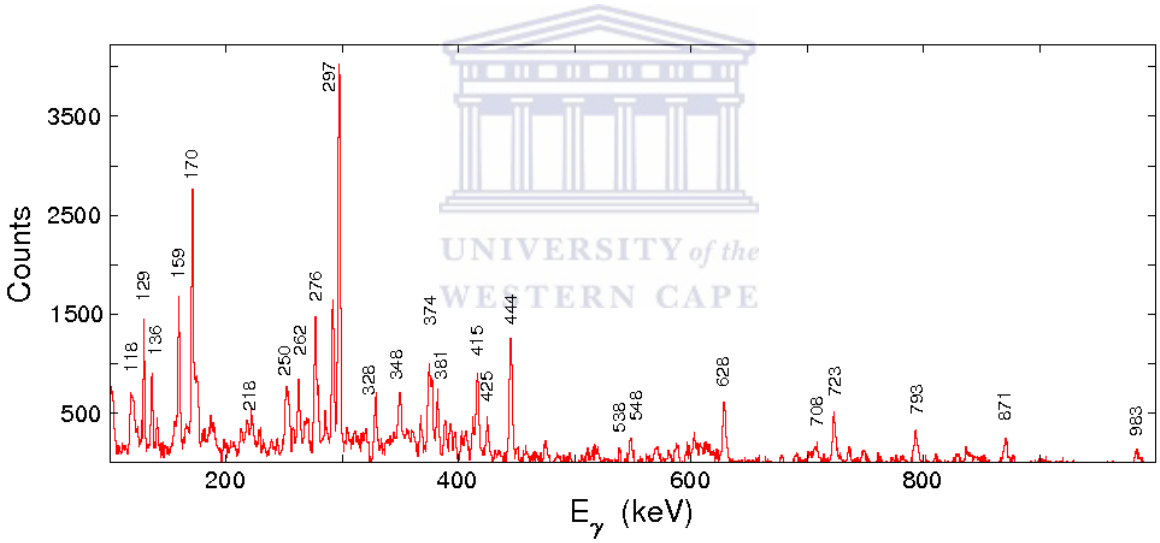

Fig 4-20 Gate set on 146 keV transition

We also see the high energy gamma ray 871 keV. Gating on 871 keV transition (as shown in Fig. 4-21) the peaks 276 keV and 262 keV appear very strongly with 146 keV, 292 keV and 159 keV transitions, etc. showing in coincidence too. It seems as if only one of the members of the 297 keV doublet transition is in coincidence with the 871 keV transition, since the 297 keV peak is very weak. Another observation to note is the energy sum 871 keV+262 keV=297 keV+836 keV. The suggested placement of one of the 297 keV transitions and the 871 keV gamma rays as is shown in Fig. 4-22. The 871 keV transition is

placed directly above the 262 keV and 276 keV transitions, linking the new structure to band 1 as shown in Fig. 4-22.

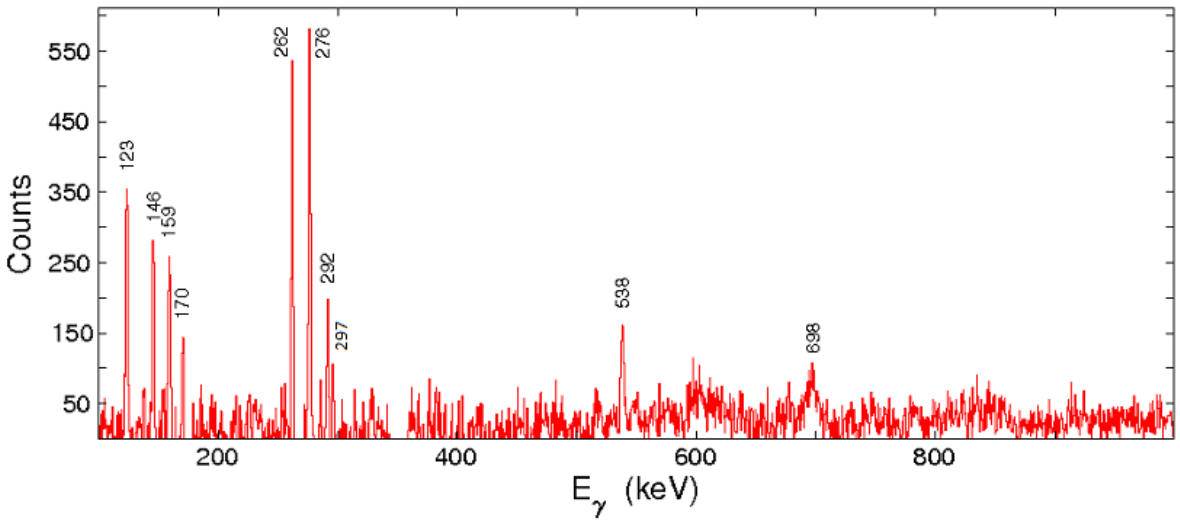

Fig 4-21 Gate on 871 keV transition

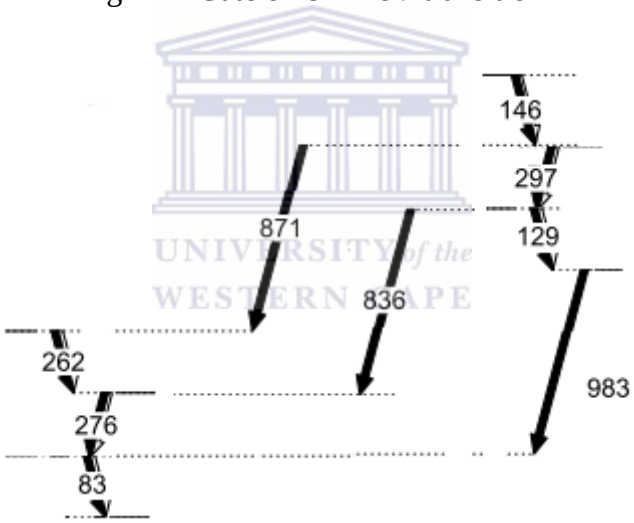

Fig 4-22 Partial level scheme showing building of the level scheme for band2

Before building the level scheme at higher excitation energies, we note the presence of the 191 keV and 252 keV transitions, which are in coincidence with several transitions of this part of band2. Furthermore 191 keV+252 keV= 297 keV+146 keV while 191 keV transition is found in anti-coincidence with 146 keV transition (see Fig. 4-20) since 191 keV transition is not seen in the spectrum gated by the 146 keV transition. Further coincidence analysis confirmed the placement of the peaks 191 keV and 252 keV in parallel to the peaks 297 keV and 146 keV (see Fig. 4-23). The peaks 170 keVand 159 keV were placed above 146 keV

transition and then the remaining transitions from band2 were placed on top. No cross-overs were found in parallel to 159 keV and 170 keV transitions, thus their order is arbitrary.

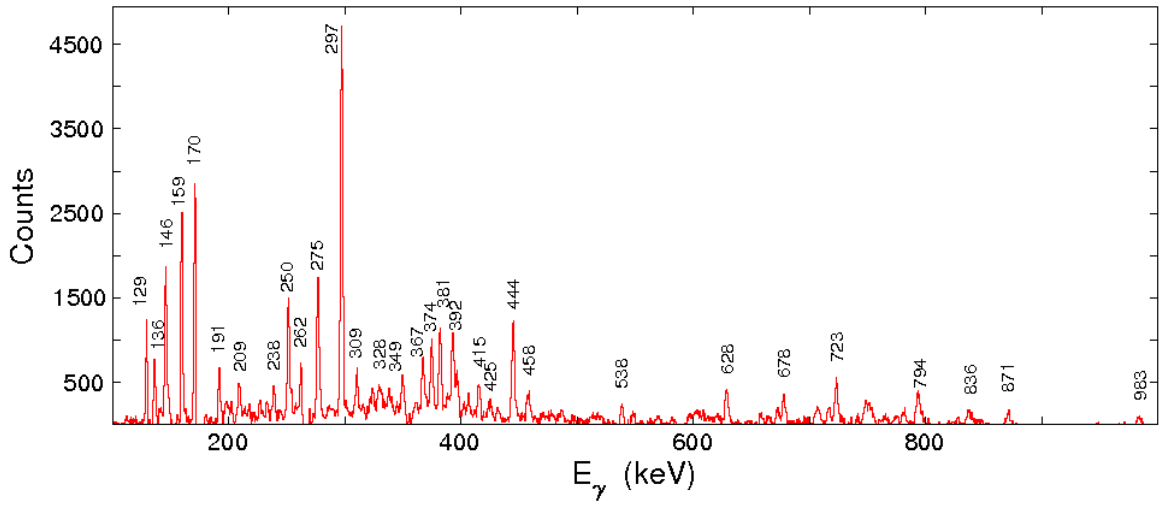

Fig 4-23 Gate on 292 keV transition

The placement of the rest of the transitions in band2 was confirmed by establishing the cross-overs, like 678 keV, 748 keV and 588 keV. The level scheme thus far is seen in Fig. 4-24.

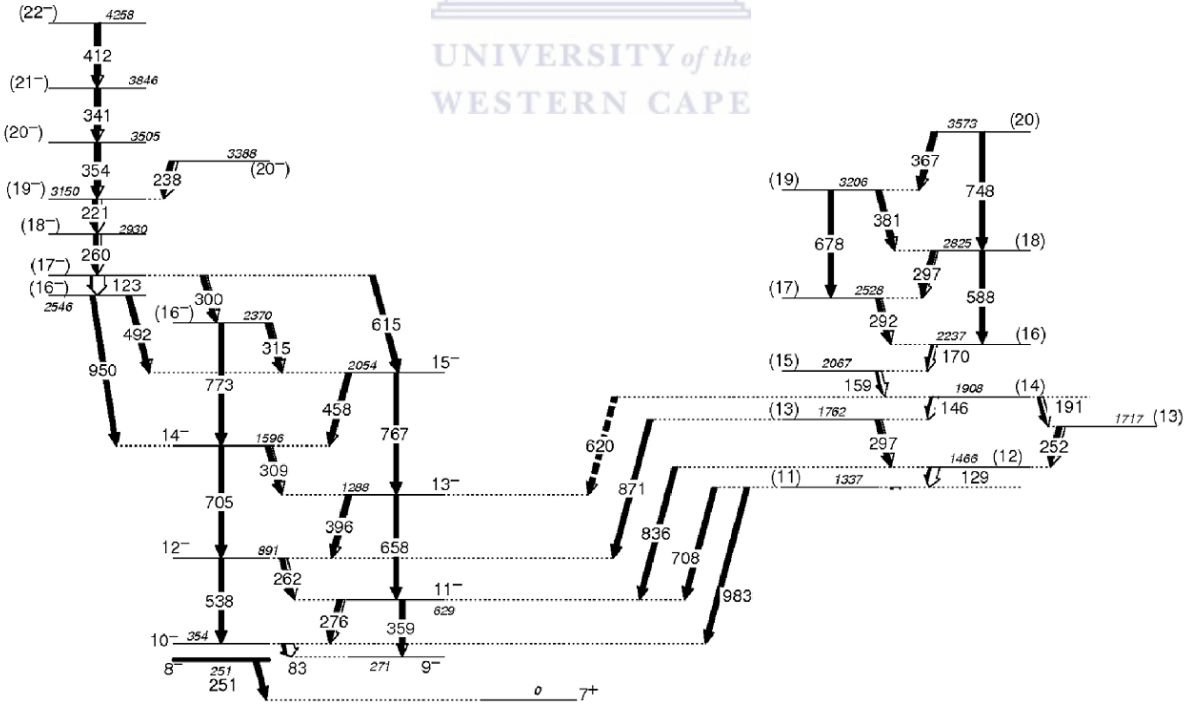

Fig 4-24The level scheme thus far showing the extension of the known level scheme (band1) and the new band2.

4.2.1.4 Other decays of band 2

Two small structures of transitions were discovered below the 129 keV gamma-ray. They are in anti-coincidence with each other. Gating on 129 keV transition (see Fig. 4-25) the peaks 136 keV, 374 keV and 444 keV are very strong. These strong peaks are not accounted for yet.

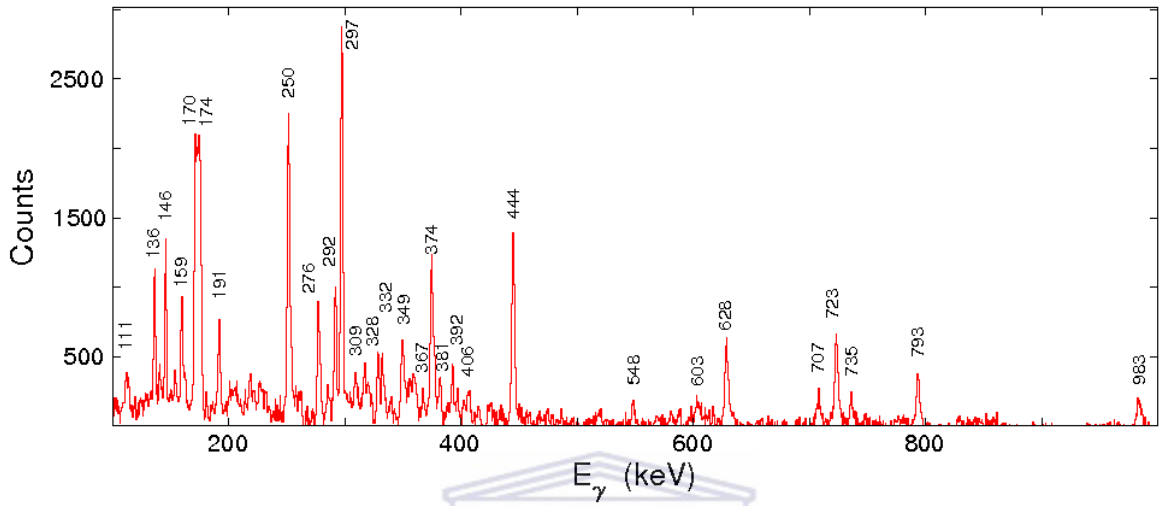

Fig 4-25 gate on 129 keV

Gating on the 444 keV transition (Fig. 4-26) we see that 136 keV, 723 keV, 374 keV and 349 keV peaks are the dominant peaks. Gating on 374 keV transition (see Fig. 4-27) the peak 723 keV disappears and a new peak 793 keV is seen. Therefore 723 keV gamma-ray should be placed in anti-coincidence with 374 keV and 793 keV transitions and should be in anti-coincidence with 444 keV. When gating on 349 keV peak (see Fig. 4-28) both 444 keV and 374 keV transitions are seen but now 793 keV and 723 keV transitions disappear. Furthermore 444 keV+349 keV=793 keV and 349 keV+374 keV =723 keV. This analysis resulted in the placement of these peaks in the level scheme as shown in Fig. 4-29.

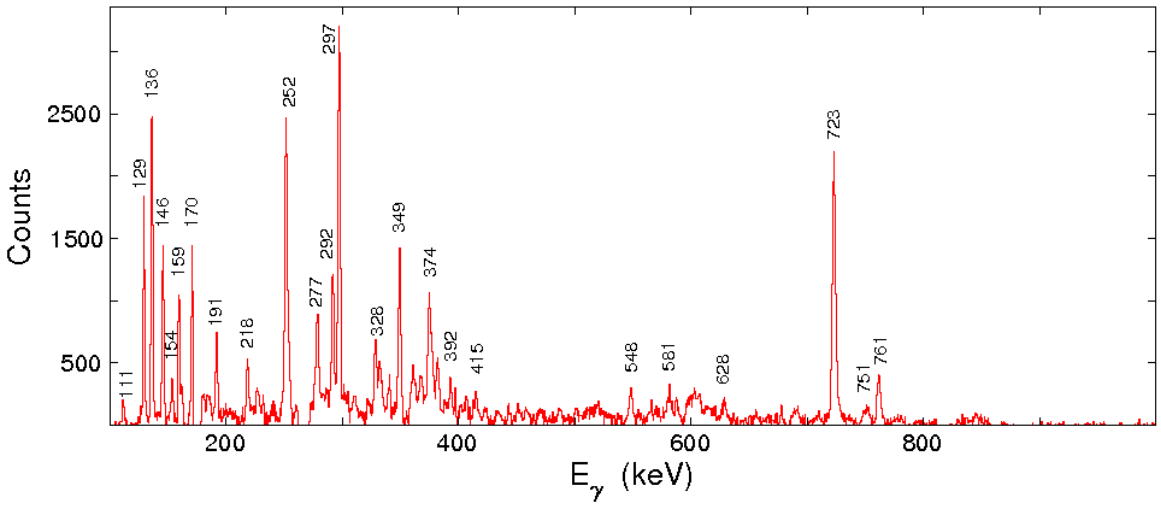

Fig 4-26 gate on 444 keV transition

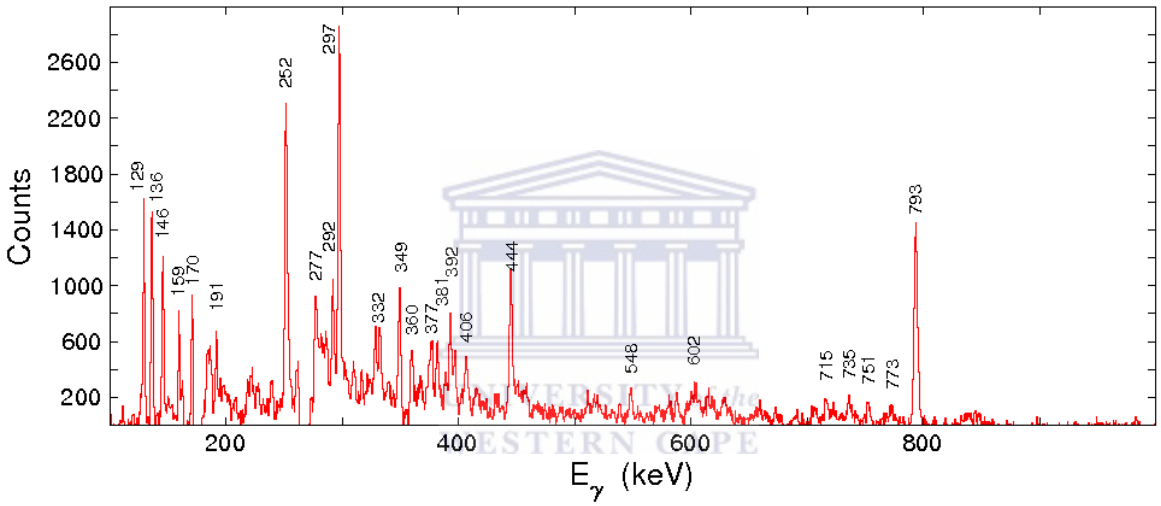

Fig 4-27 Gate on 374 keV transition

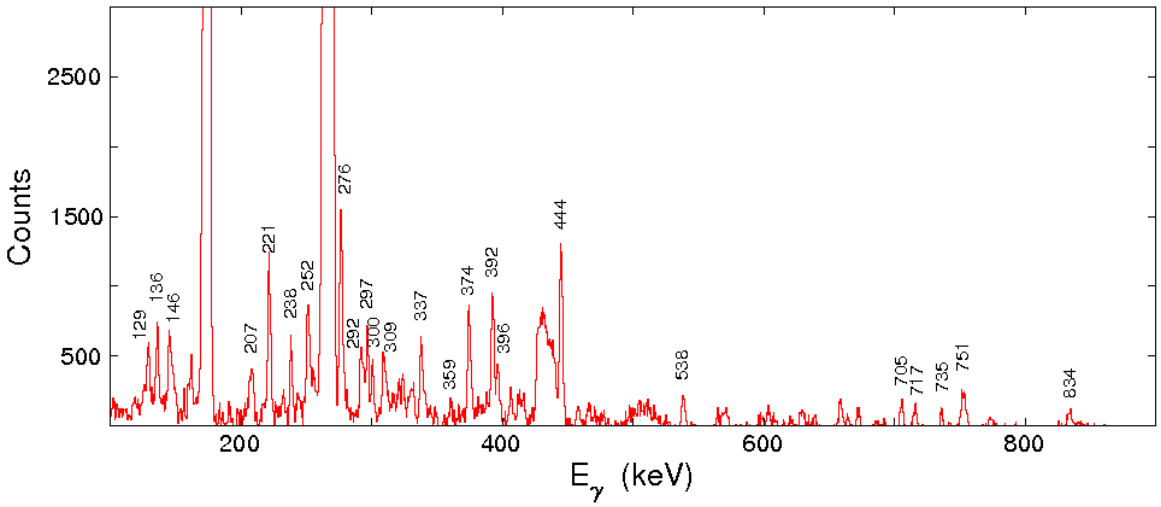

Fig 4-28 Gate on 349 keV transition

This placement is also consistent with the observation that the 136 keV, 444 keV and 374 keV transitions are in anti-coincidence with all of the high energy transitions linking band 2 to band 1,peaks like 983 keV, 836 keV and 871 keV and also with band1 gamma rays. The orientation of this structure could not be unambiguously confirmed. For instance it is possible to place 136 keV transition below the 444 keV transition. Alternatively one could turn around the placement of the gamma ray transitions in this structure. They could have been placed with the 444 keV transition directly below the 129 keV transition and rest of the transitions could be placed accordingly.

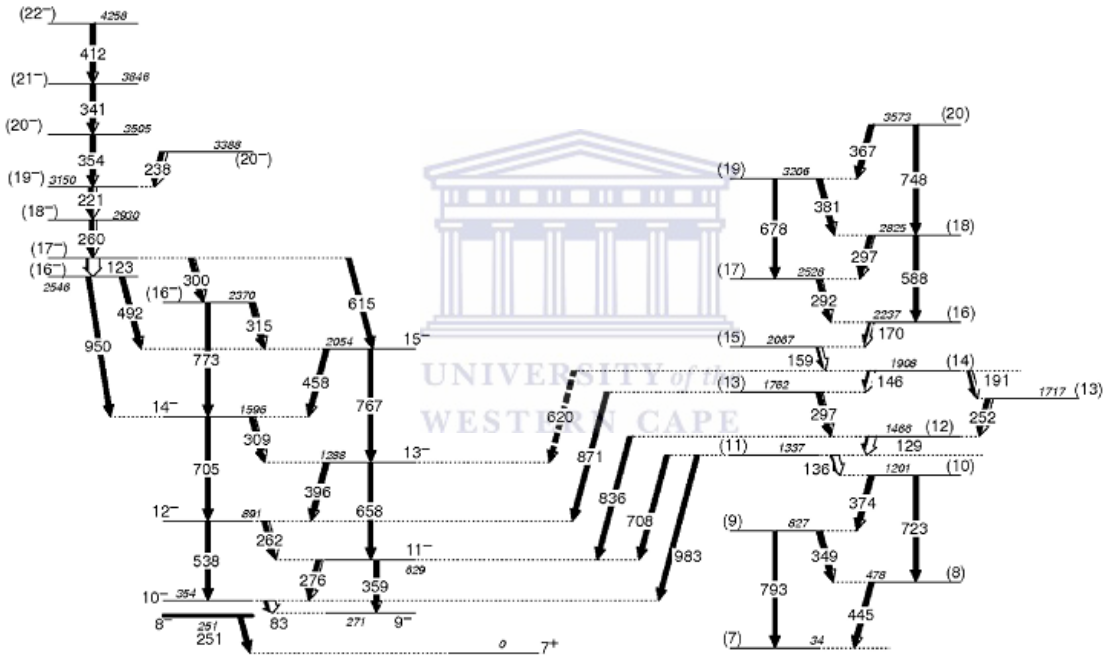

Fig 4-29 The level scheme thus far for ^{192}Tl

Another structure links the levels at excitation energies 1337 MeV and 34 keV. It consists of the 628 keV, 140 keV, 285 keV, 250 keV, 258 keV, 277 keV and 425 keV transitions. The coincidence analysis of these transition resulted in the placement shown in Fig. 4-30.

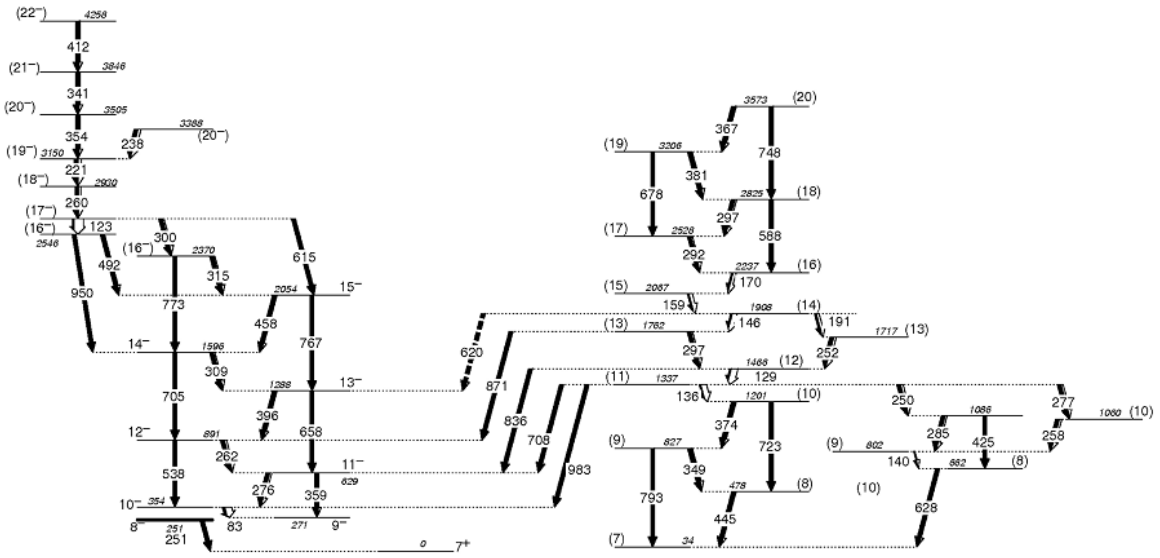

Fig 4-30 the placement of the levels below 129 keV transition

4.2.1.5 **Band3**

This band consists of 328 keV, 377 keV, 360 keV, 581 keV, 657 keV and 688 keV gamma ray transitions. Among them there is the 328 keV doublet transition. Doublets are interesting pairs of transitions because when gating on a doublet transition one observes a spectrum gated on both members of the doublet, as in the case with 328 keV transition (see Fig. 4-31).

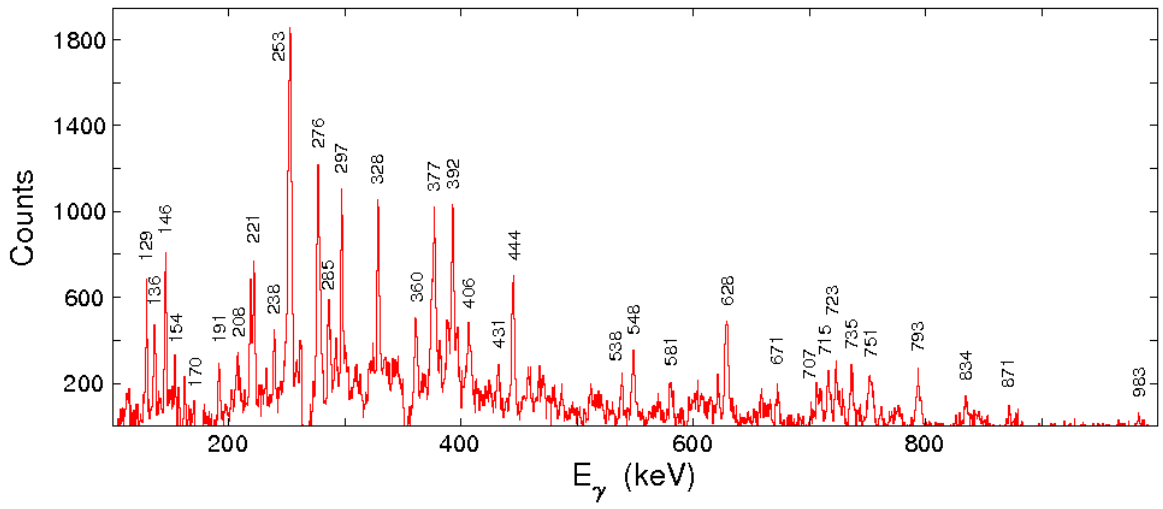

Fig 4-31The doublet transition 328 keV

One examines such spectra trying to identify close to which other gamma rays the two members of the doublet may be. Looking at Fig. 4-31 two strong peaks 253 keV and 328 keV are noticeable. One can assume as a first step that the two 328 keV and the 253 keV transitions lie close to each other. Two possible ordering of these three gamma rays are shown in Fig. 4-32. Crucially in determining the placement is the observation E2 cross-over transitions. In this case 657 keV cross-over was observed which established that the two 328 keV gamma rays were to be placed on top of each other. Studying the coincidence relationships the other transitions in band3 were placed as shown in Fig. 4-33.

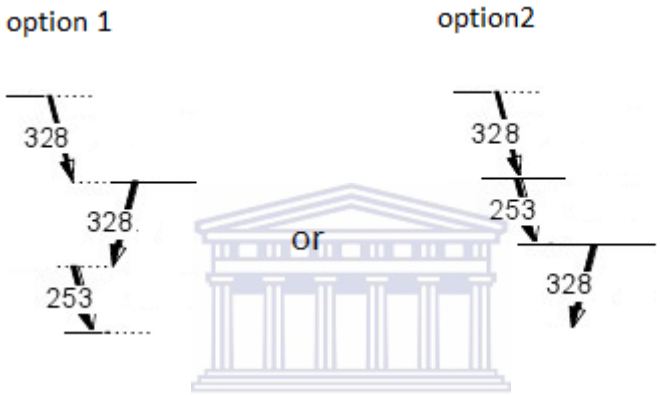

Fig 4-32 two of the several possible placements of the doublet transition 328 keV in band3

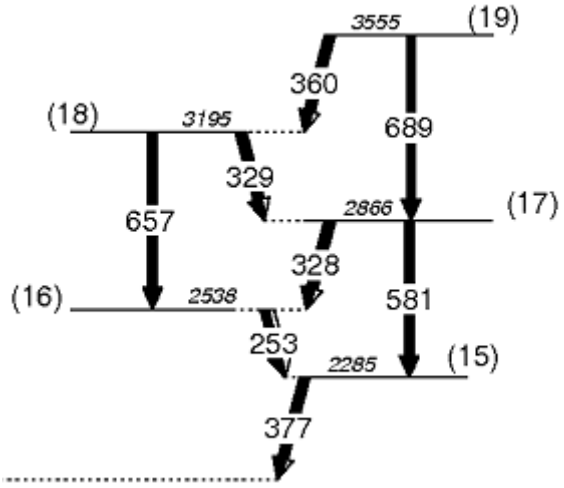

Fig 4-33 showing the placement of the doublet 328 keV, cross-over 657 keV and other coincidence transitions

4.2.1.6 Other difficult cases

Another placement that proved difficult was the 252 keV gamma-ray. These are in fact 250 keV, 252 keV and 253 keV transition all in coincidence with each other. This excludes the 251 keV transition lying below the 8^- isomer.

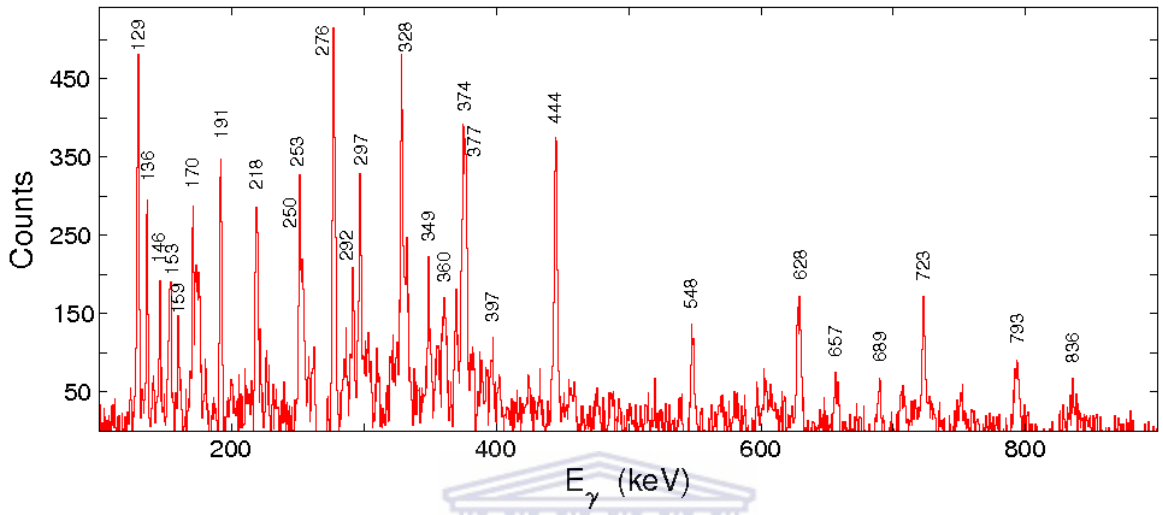

Fig 4-34 gate on 252 keV transition

In the spectrum gated on 252 keV transition (as shown in Fig 4.-34) one sees that 250-253 keV peak is not very strong, meaning that it is most likely that the members of the triplet are not in immediate proximity to each other. Crucially for the placement of this triplet, was to determine other transitions that lye close to the members of the triplet and also to observe cross-overs. In this case gating on the 253 keV member of the triplet showed an increased intensity of the 328 keV doublet transitions, when compared to the spectra gated on 252 keV and 250 keV transitions. The spectrum gated on 253 keV gamma-ray (see Fig. 4-35) shows the transitions 444 keV and 723 keV much weaker. The first assumption is that 444 keV and 723 keV transitions are much further away from the 253 keV transition. Also one notices the appearance of the 377 keV and 360 keV transitions, when gating on 253 keV gamma-ray. Thus the placement of the 253 keV transition is in band 3.

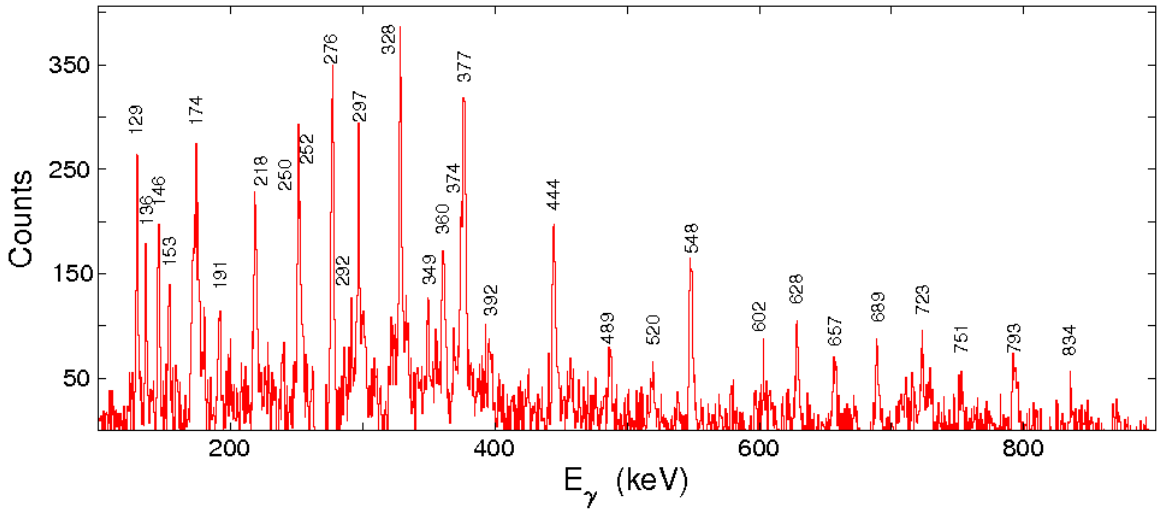

Fig 4-35 gate on 253 keV transition

4.2.1.7 **Almost doublet**

Peaks that differ by about 1-2 keV are a little easier to place, because they overlap only partly (see Fig. 4-36). This means that when gating on one of them (P2 for example) the gated spectrum shows peaks that are in coincidence with peaks P1 and P3 too. If one has to gate on P1 it is possible to obtain a clearer gated spectrum if instead of gating on the centroid of P1, one gates on the low energy side, choosing energy with say 1-2 keV lower. One problem with this method is that the peaks seen from such a gate are not as intense. But is a helpful way to see the true coincidences.

Consider the real case of peaks like 374 keV and 377 keV transitions which are in coincidence (see Fig. 4-37.

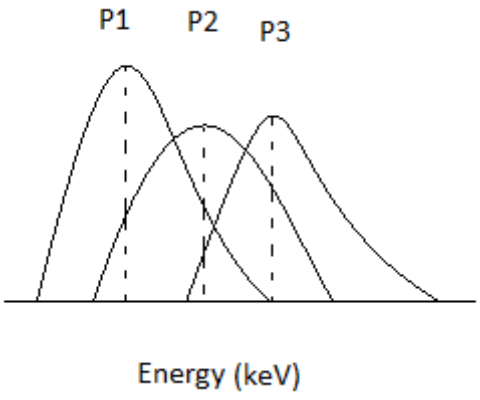

Fig 4-36 overlap of peaks that differ by 1 keV in energy

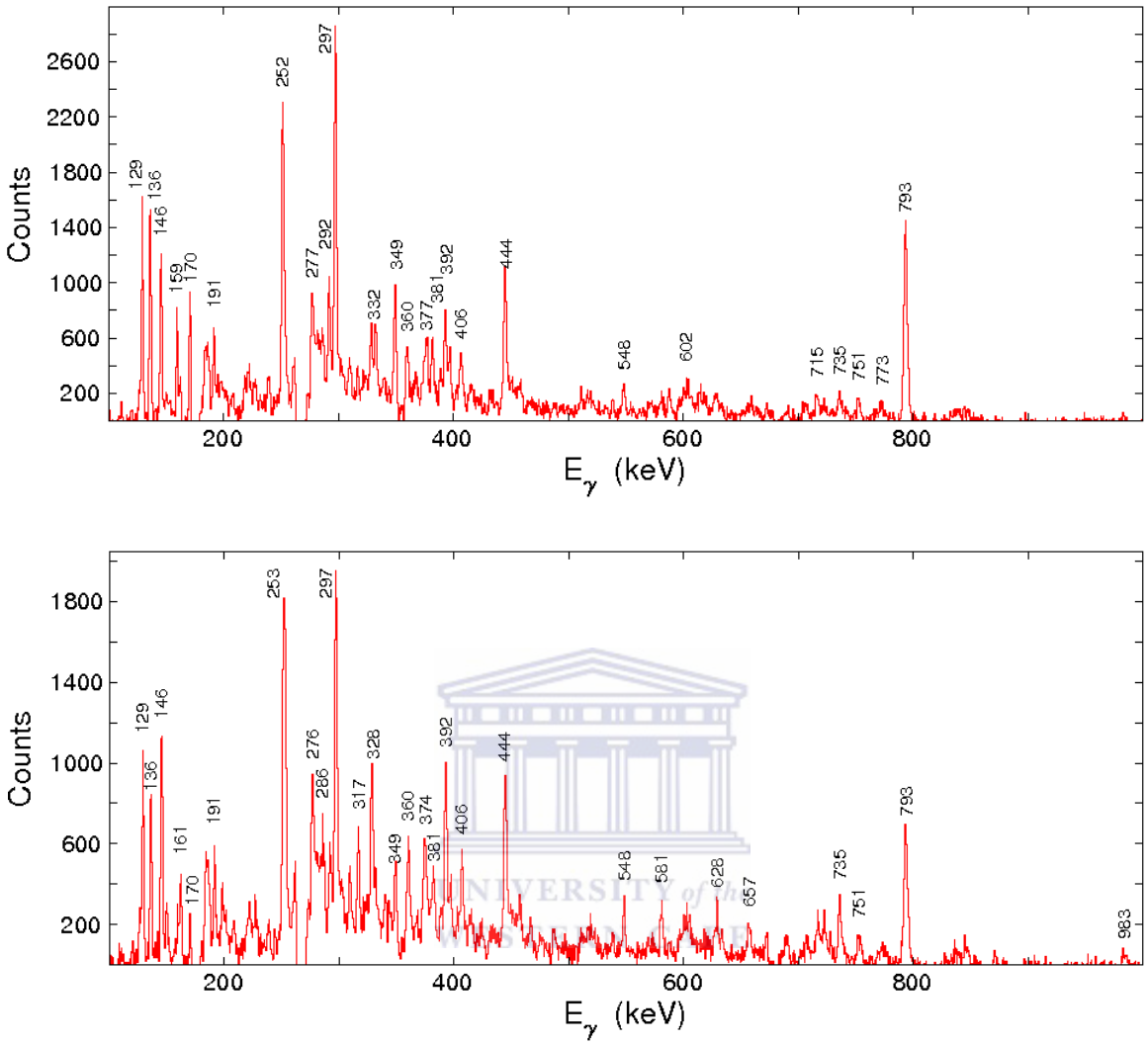

Fig 4-37 top panel is a gate on 374 keV and the bottom is a gate on 377 keV transitions

The two spectra in Fig. 4-37 look very similar but gating on 378 keV and 373 keV transitions (see Figs. 4-38 and 4-39) one can see the difference in the in coincidences with much better.

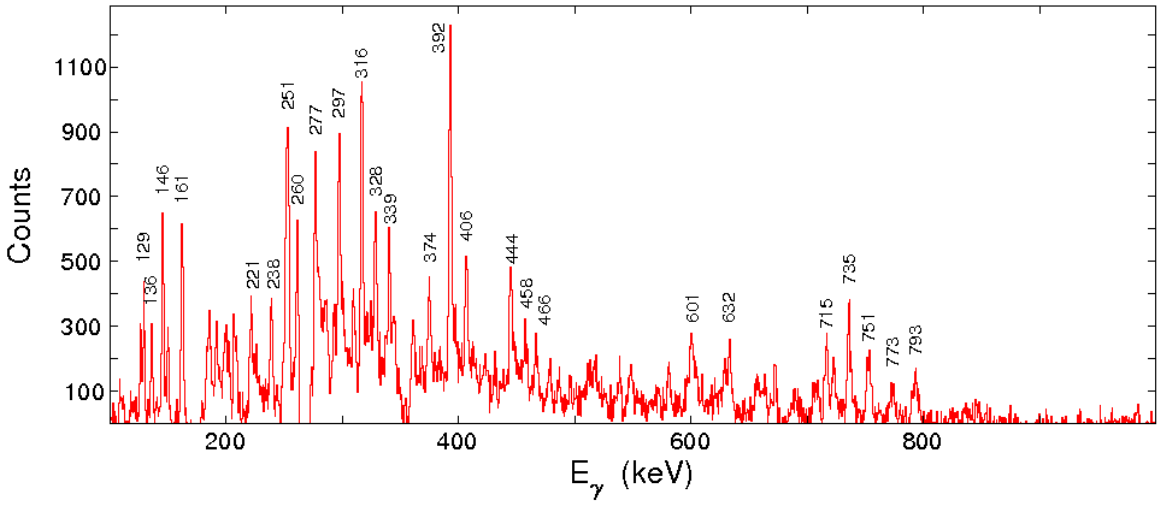

Fig 4-38 gate on 378 keV transition

When looking at Fig. 4-37 the peak 253 keV is very strong. In Fig. 4-38 this peak has a lower energy of ~252 keV. This suggests that 377 keV transition is closer to 253 keV transition while 374 keV transition is closer to 252 keV gamma-ray. The spectrum gated on 378 keV transition brings some contaminating transitions from ^{193}Tl, which need to be ignored. Another clear difference is shown in the intensities of the 349 keV and 793 keV peaks. They must be lying close to the 374 keV transition and much further away from the 377 keV transition.

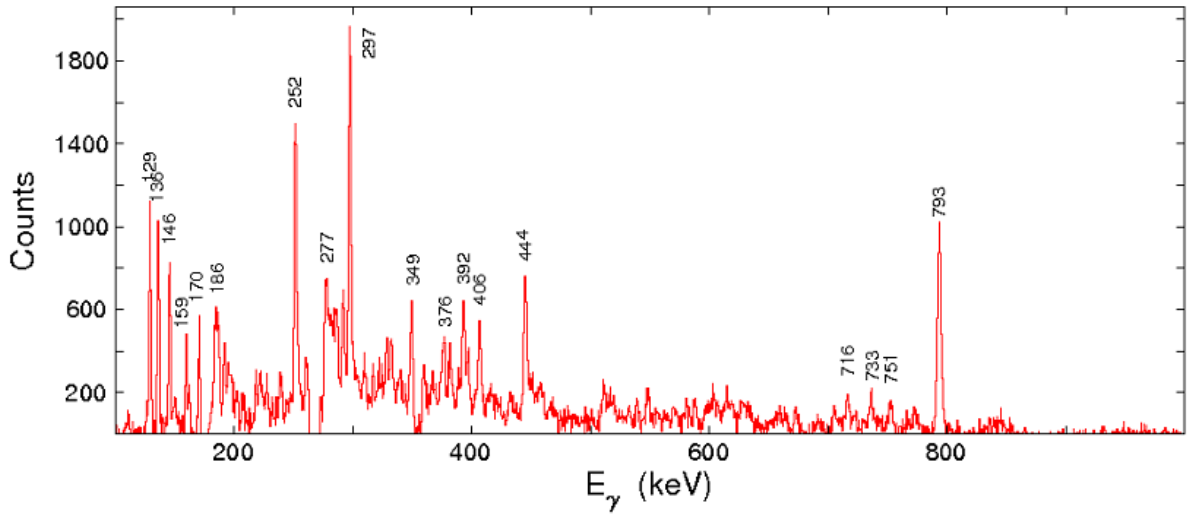

Fig 4-39 gate on 373 keV transition

4.2.1.7 The final level scheme

The final level scheme is shown in Fig. 4-40. No spins or parities were measured in this work thus the assignments in brackets are inferred from comparing with the neighbouring nuclei. In some cases, in particular the levels below the 129 keV transition, the spin assignments given in brackets are very uncertain. In the next step of the data analysis angular distribution ratios and linear polarization anisotropies and also gamma ray intensities will be measured.

It should be noted that this gamma-coincidence analysis used the data collected within the two weekends of beam time, when the thin target was used. No chiral partner band to the yrast band was discovered so far in this data. However such search will be performed again when the additional thick targets data is added.

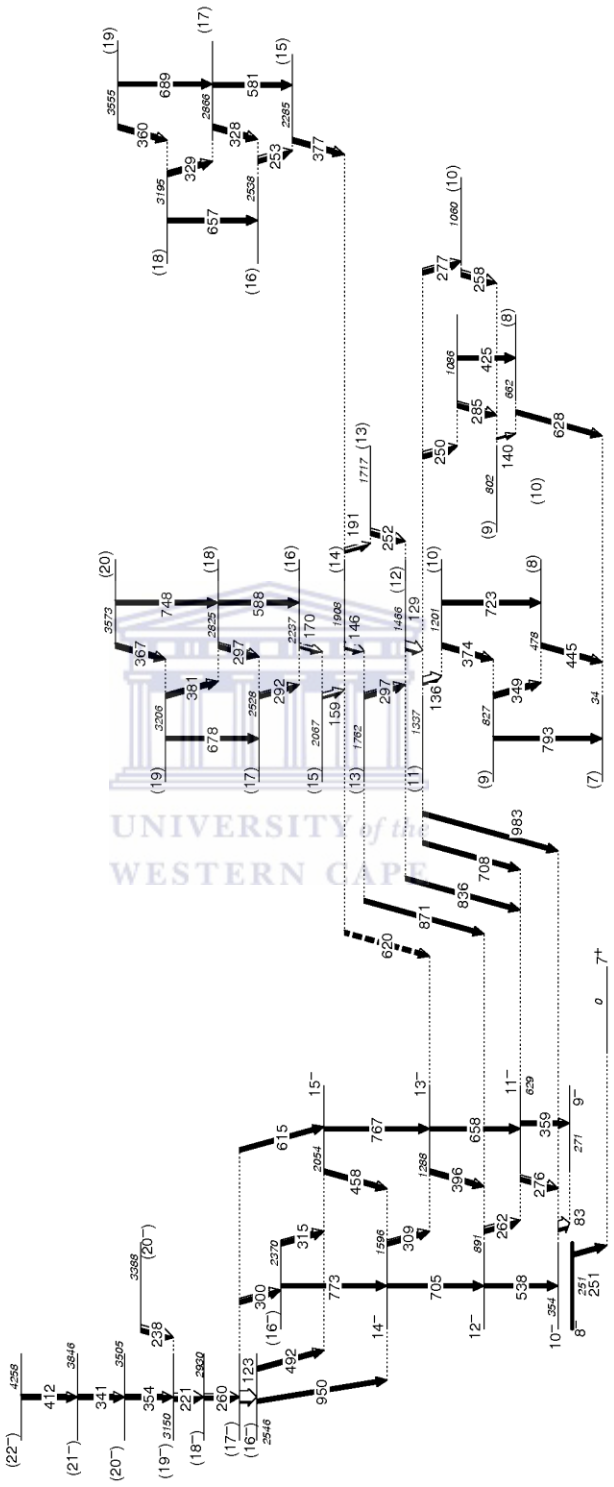

Fig 4-40 The final level scheme

4.3 Discussion and conclusion

To account for the observed structure in ^{192}Tl, deformed shell model and the PRM (particle rotor model) framework will be used.

4.3.1 Deformed Shell model

The deformed shell model is an extension of the shell model that accounts for nuclei that are not spherically symmetric.

The deformed shell model describes single particle orbits in a deformed nuclear potential. Unlike the shell model which assumes a spherically symmetric potential with no interaction between particles the deformed shell model considers deformed nuclear potential in which the particles orbit. Nucleons that are far from closed shells tend to induce deformed nuclear shapes. The nuclei may get into axially symmetric deformed shapes (prolate or oblate) or triaxial shapes.^{192}Tl has Z=81 and N=111 with one proton short to fill the 82 shell and 15 neutrons away from filling the 126 shell. With an excess of 15 neutron holes in between closed shells, the shape of this nucleus becomes moderately deformed.

To construct the deformed shell model Hamiltonian several terms are needed. These include the isotropic harmonic oscillator potential $\hat{H}_o = -\frac{\hbar^2}{2M}\nabla^2 + \frac{1}{2}M\omega_o^2 r^2$, which describes the spherically symmetric nuclear potential well. In our case the orbiting nucleons move in a deformed potential. To account for this a term introducing quadrupole deformation is added. The shape of the potential is proportional to the quadrupole field and is given by

$$\hat{H}_d = -\delta M\omega_o r^2 \frac{4}{3}\sqrt{\frac{\pi}{5}}Y_{2\,0} = -M\omega_o r^2 \beta Y_{2\,0},$$

Where β is the deformation parameter, δ is the shaping parameter and $Y_{2\,0}(\theta,\phi) = \frac{1}{4}\sqrt{\frac{15}{2\pi}}(3cos^2\theta - 1)$. The deformation parameter is related to the quadrupole moment Q_o and tells us whether the nucleus is prolate or oblate in shape. To a first approximation the quadrupole moment Q_o is given by

$$Q_o \cong \frac{3}{\sqrt{5\pi}}R_{av}^2 Z\beta \qquad (4.1).$$

When $\beta < 0$ the nucleus is oblate and when $\beta > 0$ it is prolate. A zero quadrupole moment occurs when the nucleus has spherical charge distribution. An important term in the interaction is the spin orbit coupling $\hat{H}_{so} = C\vec{l}\cdot\vec{s}$ of the orbital angular momentum and the spin of the nucleon, where C is the strength of this coupling. This effect splits the subshell (except $s_{1/2}$) into two, e.g. $h_{9/2}$and $h_{11/2}$. A shaping term is also needed to create an intermediate potential between the square well and the harmonic oscillator potentials, and this force is given by $\hat{H}_s = D\vec{l}^2$, where D is a parameter that simulates the deviation from a oscillator potential to a more realistic one. Therefore the single particle Hamiltonian of the deformed well is the sum of the following terms,

$$\hat{H} = \hat{H}_{sp} = \hat{H}_o + \hat{H}_d + \hat{H}_{so} + \hat{H}_s - \frac{\hbar^2}{2M}\nabla^2 + \frac{1}{2}M\omega_o^2 r^2 \; - M\omega_o r^2 \beta Y_{2\,0} + C\vec{l}\cdot\vec{s} + D\vec{l}^2.$$

To find the wave functions one writes

$$\hat{H}\varphi_{\Lambda\Omega} = \left(-\frac{\hbar^2}{2M}\nabla^2 + \frac{1}{2}M\omega_o^2 r^2 \; - M\omega_o r^2 \beta Y_{2\,0} + C\vec{l}\cdot\vec{s} + D\vec{l}^2\right)\varphi_{\Lambda\Omega} = E_{\Lambda\Omega}\varphi_{\Lambda\Omega}\,,$$

which has a solution $\varphi_{\Lambda\Omega} = |N\Lambda\Omega> = \sum_{Nlj} a_{Nlj}\,|Nlj>$ in terms of the spherical bases states.

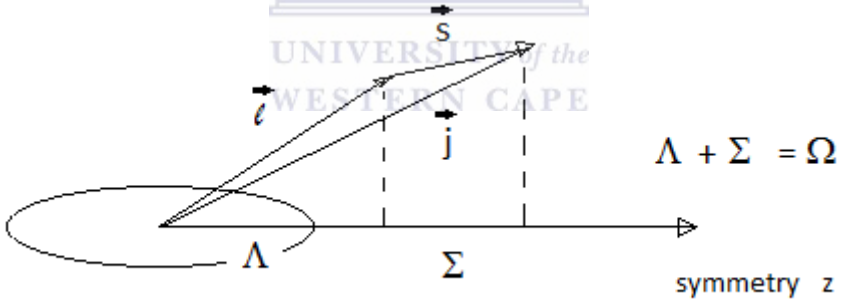

Fig 4-41 Nilsson quantum number Ω

Here Λ is the projection of $\vec{l}$ along the symmetry (z)axis, Σ is the projection of $\vec{s}$ along the z axis,Ω is the projection of $\vec{j}$ along the z axis, N is the principal number of the major shell and a_{Nlj} are the Clebsch-Gordon coefficients. New quantum numbers are needed, because of the mixing of shell model levels the old quantum numbers like l=3 for the $f_{7/2}$ state are not conserved. The $f_{7/2}$ state has j=7/2 at a spherical shape and splits into levels with projections $|\Omega| = j, j-1, \ldots 1/2$ when the shape becomes deformed, i.e. four levels since |Ω|>0, for

which j is not a good quantum number. Thus, one of the new good quantum numbers is the projection Ω. The same goes for $\Lambda = \Omega - \Sigma$.

The single particle energy of a deformed state for axially symmetric shapes is given by

$$E_{\mathrm{N}} = \left(n_z + \frac{1}{2}\right)\hbar\omega_z + (n_{x+y} + \frac{1}{2})\hbar\omega_{x+y},$$

where $N = n_{x+y} + n_z$,$n = 0, 1, 2, \ldots$,

$$\omega_{x+y} = 2\omega_o\sqrt{(1 + (\tfrac{4}{5}\pi)^{1/2}\beta)}\text{and}\omega_z = 2\omega_o\sqrt{(1 - 2(\tfrac{4}{5}\pi)^{1/2}\beta)}.$$

The single particle energy levels are conveniently plotted in the Nilsson diagrams as a function of β for protons and neutrons (as shown in Fig 4-42).

The Nilsson diagrams for protons and neutrons are different. This is because of the Coulomb repulsion the protons feel. The Coulomb force modifies the potential depth increasing the Fermi energy for protons. The Fermi energy level is the highest level which is filled with the available number of protons or neutrons, assuming that the nucleus has zero excitation energy. ^{192}Tl is a deformed nucleus. Experimentally it is usually the spectroscopic quadrupole moment Q that is measured (this is the quadrupole moment when measured in the laboratory frame) while the intrinsic quadrupole moment Q_o reflects the nuclear quadrupole deformation. These two quadrupole moments are related by

$$Q = \frac{3K^2 - I(I+1)}{(I+1)(2I+3)}Q_o \qquad (4.2),$$

where I is the nuclear spin and K is the projection of I on the symmetry axis.

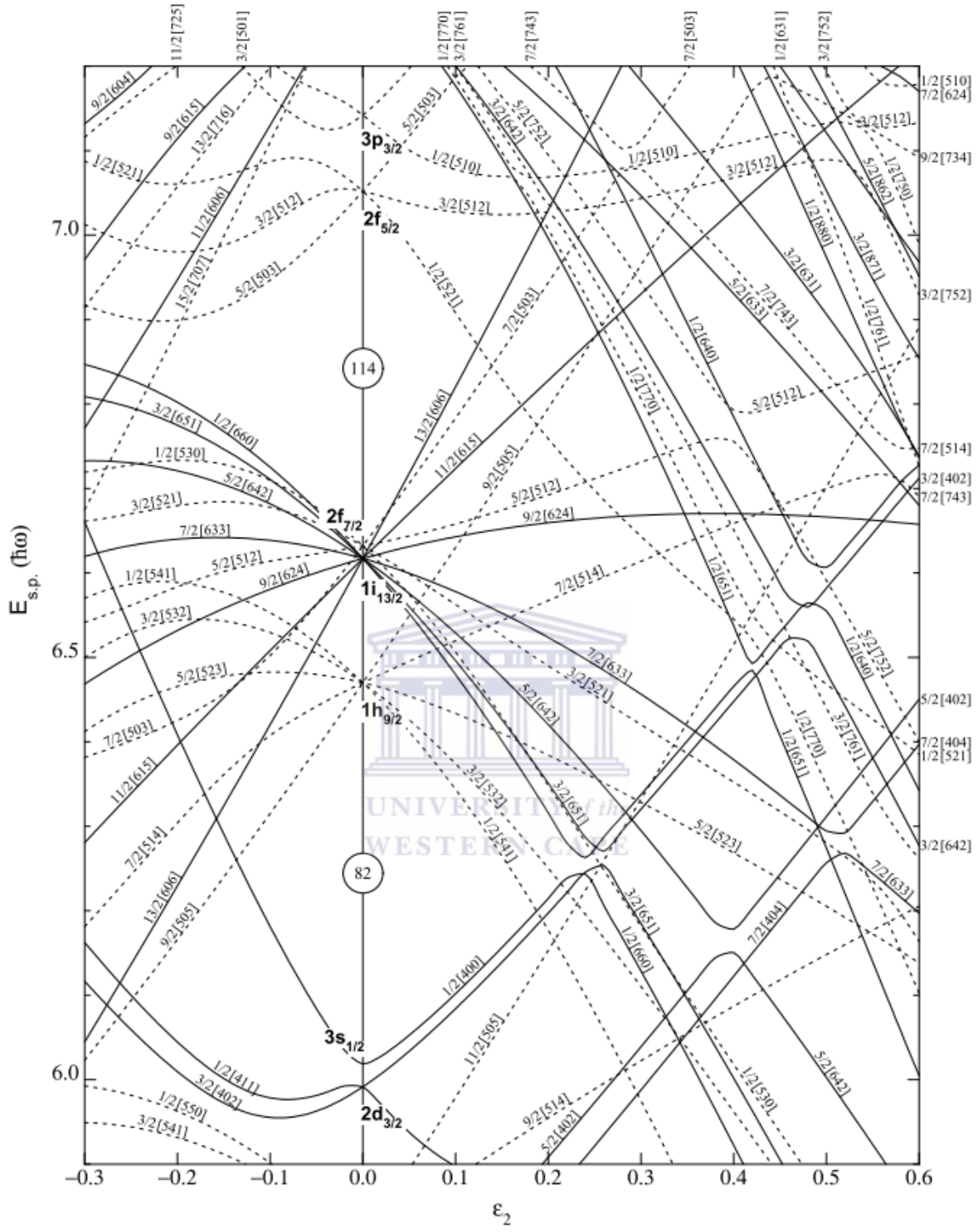

Fig. 4-42a Nilsson diagram for protons 50≤Z≤82 [Nil12]

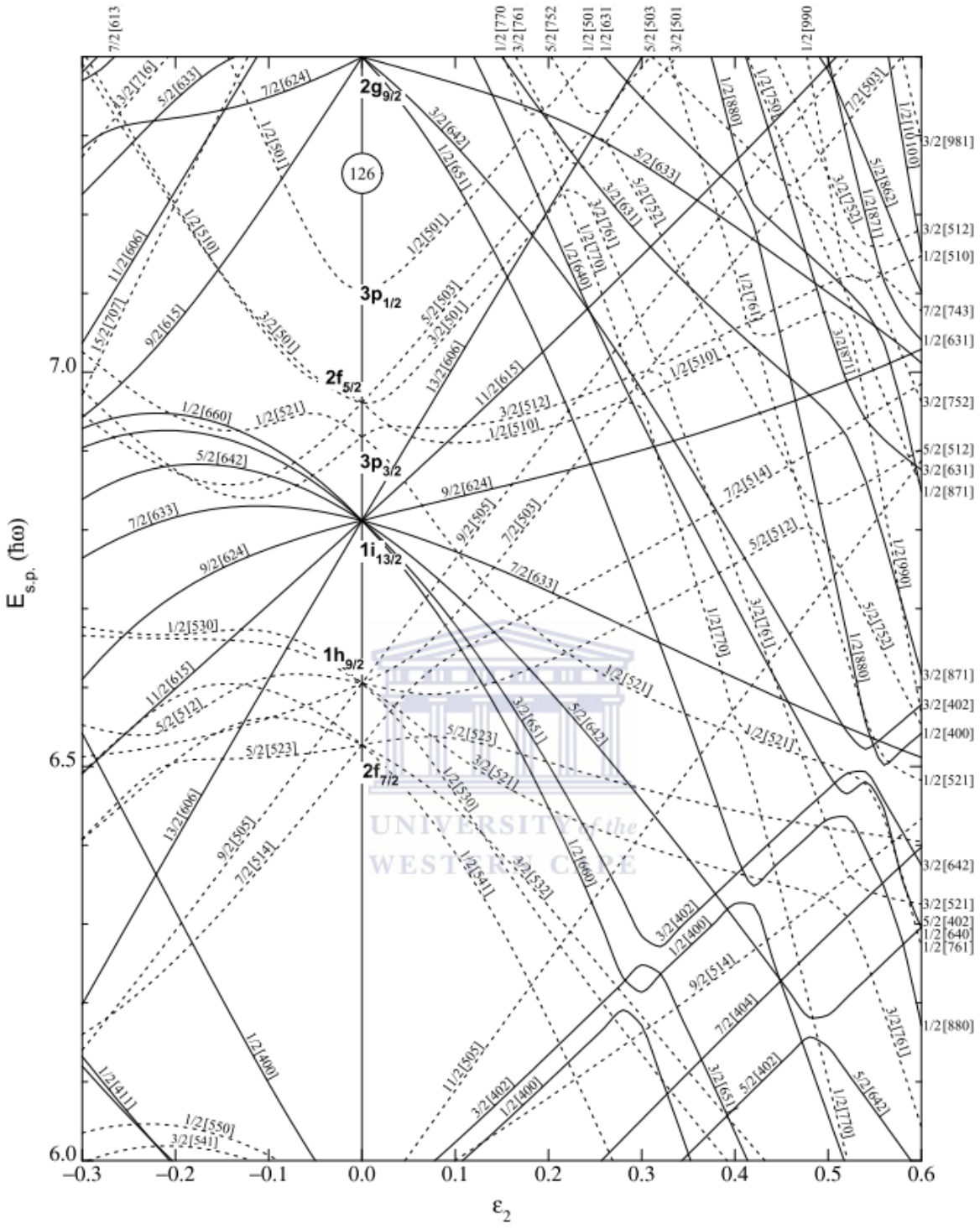

Fig 4-42b Nilsson plot for neutrons 82 ≤N ≤126[Nil12]

4.3.2 **Band1**

In ^{192}Tl the rotational bands are based on the $I^{\pi} = 8^{-}$ state, thus this state is of prime interest. The actual ground state in ^{192}Tl is an isomer 2^{-} (lifetime =9.6 min) that undergoes positive beta decay or electron capture to ^{192}Hg. ^{192}Tl has 81 protons and oblate deformed shape. Looking at the Nilsson diagram for protons, this makes the Fermi level for protons to lie at the bottom of the $h_{9/2}$ shell, which means that the unpaired proton will occupy an orbital originating from the $h_{9/2}$ shell. Similarly the Fermi level for neutrons lies at the top of the $i_{13/2}$ shell, i.e. the unpaired neutron occupies an orbital originating from the$i_{13/2}$ shell.

Since ^{192}Tl is rotating (deformed nuclei can be observed to rotate while spherical nuclei cannot) the PRM (particle rotor model) can be used. The wave functions are then given by $\Psi = \varphi_{\Lambda\Omega} \cdot \Phi_{rot}$, where $\varphi_{\Lambda\Omega}$ are the intrinsic deformed wave functions and Φ_{rot} are the rotational wave functions of the nucleus in the laboratory frame. The new rotational Hamiltonian is

$$\hat{H} = \hat{H}_{\text{sp}} + \hat{H}_{\text{rot}},$$

where

$$\hat{H}_{\text{rot}} = \frac{\hbar^2}{2\mathcal{J}}(I^2 + j^2 - 2\vec{I} \cdot \vec{j}).$$

The Coriolis term $\vec{I} \cdot \vec{j}$, when sufficiently strong, tends to align the angular momentum of the unpaired nucleons towards the rotational axis, which is perpendicular to the symmetry axis.

Looking at the neighbouring nuclei one can get a hint as to how the odd proton and neutron in ^{192}Tl will behave. Looking at ^{191}Hg (which has Z=80 and N=111) one can examine the coupling of the unpaired neutron as the nucleus is an isotone of ^{192}Tl and has the same Fermi level as in ^{192}Tl. One can note that similar quadrupole deformation is expected in both isotones. The ground state band in ^{191}Hg is shown in Fig. 4-43 and one can see that this band is built of E2 transitions above a band head spin $I^{\pi} = 13/2^{+}$ and therefore decoupled.

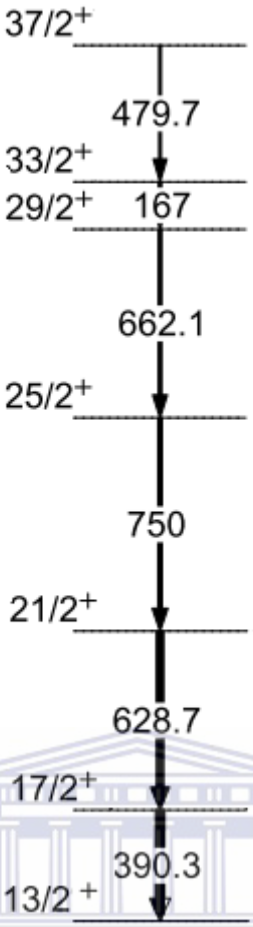

Fig 4-43Yrast band in ^{191}Hg, showing decoupled structure. The band is assigned to $\nu 1i_{13/2}$ configuration.

Decoupled band occurs when the odd neutron moves independently from the rotating core. The energies of the levels in the band are given by as

$$E(I) = \frac{\hbar^2}{2\mathcal{J}}[(I-j)(I-j+1)] \qquad (4.3),$$

where I is the spin of the state and j is the total angular momentum of the odd neutron. The band head has spin I=j and parity determined by the configuration of the odd neutron. Since the neutron occupies a level originating in the $i_{13/2}$ shell, this decoupled band starts at $I^{\pi} = 13/2^{+}$.

On the other hand ^{193}Tl has an odd proton and exhibits the rotational band shown in Fig. 4-44. This band is a strongly coupled band. Strongly coupled bands occur when the odd proton couples its motion to the rotation of the core. This happens when the angular momentum of

the odd nucleon has a large projection along the symmetry axis, and for low rotational frequencies where the Coriolis force is not very strong. The energy levels are given by

$$E(I) = \frac{\hbar^2}{2\mathcal{J}}[(I(I+1) - K^2](4.4),$$

where K is the projection of the total angular momentum along the symmetry axis.

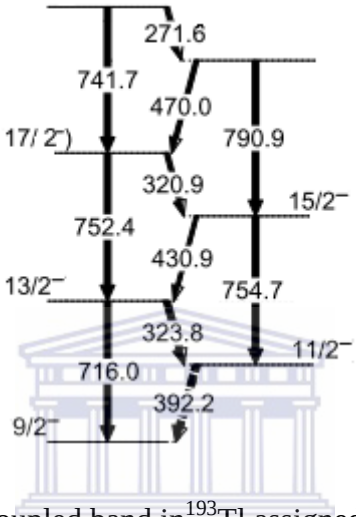

Fig 4-44Yrast strongly coupled band in[193]Tl assigned to $\pi h_{9/2}$ configuration.

Since [191]Hg is a neighbouring isotone and [193]Tl is an isotope of [192]Tl we expect that in [192]Tl there will be a similar coupling of the two unpaired nucleon states, i.e. $\pi 1h_{9/2} \otimes \nu 1i_{13/2}$. The yrast rotational bands tarts at the 8^- level. This is exactly what one gets when considering the $\pi 1h_{9/2} \otimes \nu 1i_{13/2}$ configuration. The angular momenta of the two nucleons are virtually perpendicular since $\pi 1h_{9/2}$ has projection $\Omega_p = 9/2$ along the symmetry axis and $\nu 1i_{13/2}$ has projection $\Omega_n = 1/2$. Depending on the strength of the Coriolis force the neutron can be strongly coupled or decoupled. In this case, as confirmed by the properties of the band in [191]Hg isotone the neutron angular momentum is decoupled. That means Ω_n is not a good quantum number but the projection of the angular momentum along the rotational axis, i_n is. This coupling of the two angular momenta is illustrated in Fig. 4-45. Therefore the band head spin can be calculated as:

$$I_o \approx \sqrt{(\Omega_p)^2 + (\mathrm{i}_n)^2} \qquad (4.5)$$

$$\approx \sqrt{\left(\frac{9}{2}\right)^2 + \left(\frac{13}{2}\right)^2} \approx 8.$$

Configurations like the $\pi 1h_{9/2} \otimes \nu 1i_{13/2}$ configuration in ^{192}Tl are in principal suitable for forming a chiral system. The necessary requirement for a chiral system is to have three perpendicular angular momentum vectors. The proton and neutron in the $\pi 1h_{9/2} \otimes \nu 1i_{13/2}$ configuration provide two orthogonal angular momenta. Thus the only remaining requirement is to have the rotational angular momentum pointing in the perpendicular direction to the proton and neutron angular momenta (see Fig. 4-46). This will occur if the nuclear shape is triaxial.

In principal the coupling of the two angular momenta with good projections along the symmetry axis of Ω_p and Ω_n results in a total K value, $K_{tot} = \Omega_p \pm \Omega_n = 4 \; or \; 5$.

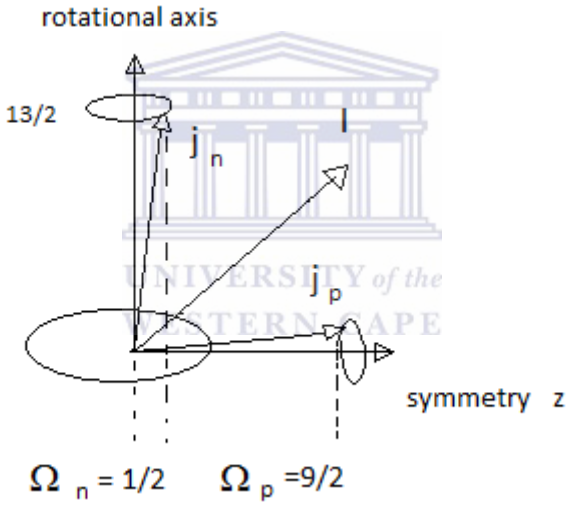

Fig 4-45 Perpendicular coupling of the proton and neutron angular momenta in ^{192}Tl

Inserting $K_{tot} = 4$ and $I = 8$ into (4.2) and using the measured quadrupole moment Q for the 8^- level in ^{192}Tl one can estimate the intrinsic quadrupole moment Q_o:

$$0.44\text{eb} = Q = \frac{3 \cdot 4^2 - 8(8+1)}{(8+1)(2 \cdot 8+3)} Q_o = -0.14 Q_o.$$

Therefore $Q_o = -3.143$ eb. Now with the aid of equation (4.1)

$$-3.143 = \frac{3}{\sqrt{5\pi}} R_{av}^2 Z \beta.$$

Solving this for β gives

$$\beta = \frac{-3.143}{\frac{3}{\sqrt{5\pi}} \cdot 81 \cdot (1.2 \cdot 192^{1/3})^2} = -0.11,$$

which is the quadrupole deformation if the nuclear shape is axially symmetric. In the published literature quadrupole deformation of 0.13-0.17 was applied for the neighbouring thallium and mercury isotopes in the 190-194 mass range which was also used.

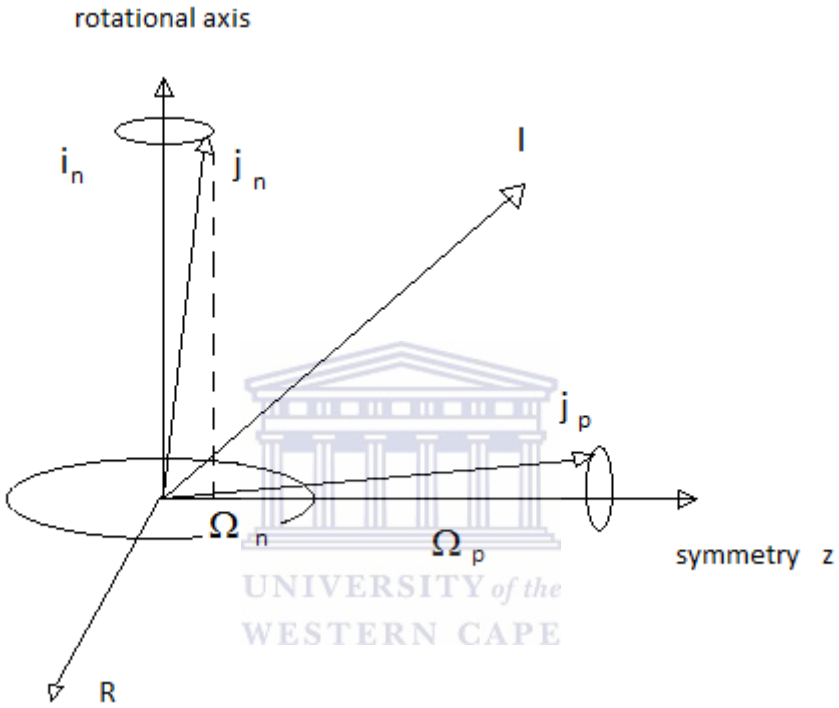

Fig 4-46 Chiral system formed by three orthogonal angular momenta

The level energy and spin in band1 increases due to the rotation of the nucleus. This band consists of the levels with $I = 8, 9, 10, \ldots$ up to 16^- for ^{192}Tl. At this point the band crossing occurs as is indicated by the decreasing energy of the 615 keV E2 transition.

4.3.3 Band4

At increased rotational angular momentum and rotational energy the Coriolis force increases. The Coriolis force increases to a point at which a pair of neutrons is broken.

One can examine bands in neighbouring mercury and thallium isotopes in order to find out more about the pair breaking. First, one notices that in neighbouring nuclei it is a neutron pair

that breaks first. The two neutrons may both occupy $i_{13/2}$ orbitals and then the band has the same parity as the yrast band.

For example in ^{195}Tl a pair breaks and the two neutrons occupy $i_{13/2}$ orbitals (see Fig. 4-48).

When a neutron pair is broken in the $i_{13/2}$ shell, it is not possible that both neutrons to occupy the $1/2^+$ [660] orbital since the Pauli principal forbids two fermions with the same quantum numbers. Thus the second neutron settles in the $3/2^+$ [651] Nilsson orbital with projection K =3/2 along the symmetry axis (see Fig. 4-47). But the Coriolis force is strong and aligns the two neutrons along the rotational axis, giving a characteristic alignment of13/2+11/2 = 12^-, fig 4-47. Since in ^{195}Tl the two neutrons are coupled with the odd proton $\pi 1h_{9/2} \otimes \nu 1{i_{13/2}}^2$ the band head spin of these rotational bands will be $I = \sqrt{(9/2)^2 + (12)^2} = 25/2$, with parity of $\pi_p \cdot \pi_n^2 = -1 \cdot (+1)^2 = -1$. Indeed this is observed in ^{195}Tl (see Fig. 4-48).

Consider another example in neighbouring ^{191}Hg isotone a neutron pair breaks, with both $i_{13/2}$ neutrons aligning along the rotational axis. This is indicated by the gain in the alignment at the band crossing (see Fig 4-41). This makes aligned three odd $i_{13/2}$ neutrons. The third neutron cannot have the same projection as the other two and thus the third neutron settles in the positive parity $7/2^+$[633] orbital. Coriolis force aligns all three neutrons along the rotational axis with alignments of 13/2, 11/2, and 9/2 (see Fig. 4-50). Therefore the band head spin of this decoupled band in ^{191}Hg will be I= j=13/2 + 11/2 + 9/2 = 33/2 (see Fig. 4-43).

In ^{195}Tl these three neutrons will be coupled with the odd proton $\pi 1h_{9/2} \otimes \nu 1{i_{13/2}}^3$ (see Fig. 4-49). One would thus expect a rotational band built on a level with spin

$$I = \sqrt{\left(\frac{33}{2}\right)^2_n + \left(\frac{9}{2}\right)^2_p} = 17$$

and with negative parity.

An interesting point to note is that band 4 seems to start at a slightly lower spin. In our case a more detailed experimental measurements need to be done on this band to confirm the actual spin.

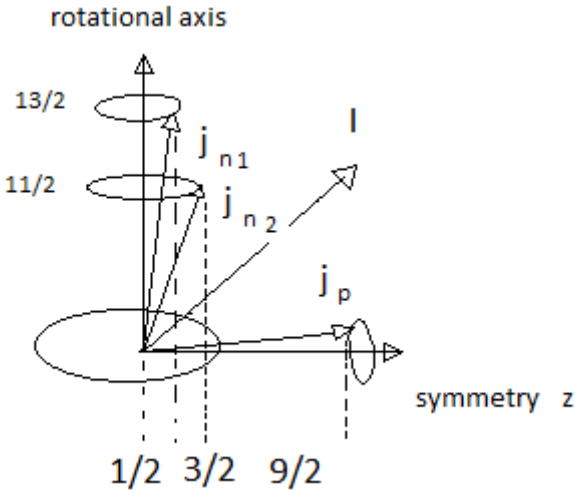

Fig 4-47 The alignment of two neutrons along the rotational axis

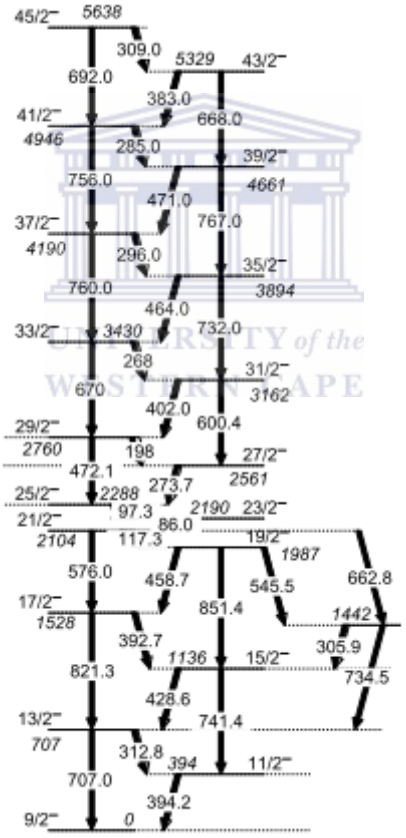

Fig 4-48 Showing the band due to the alignment of the two $i_{13/2}$ neutrons in ^{195}Tl (it has

$$I = \sqrt{(9/2)^2 + (12)^2} = 25/2)$$

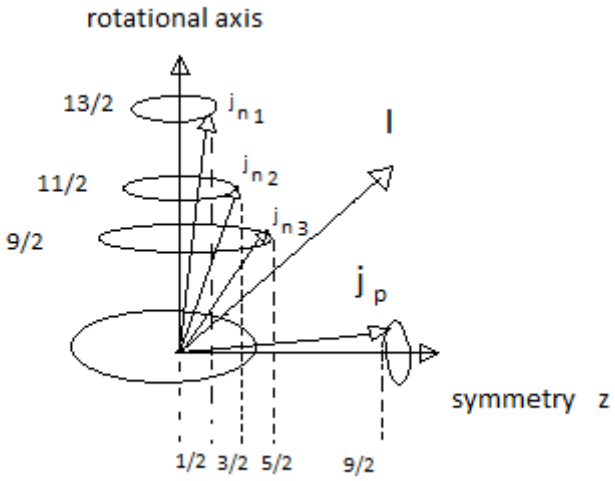

Fig 4-49 The alignment of three $i_{13/2}$ neutrons along the rotational axis coupled to an odd proton $h_{9/2}$

4.3.4 **Band2 and band3**

Going back to ^{195}Tl as a comparison, band 2 in Fig.4-40 looks similar to the positive parity band of ^{195}Tl (see Fig. 4-50). The positive parity band comes when one of the unpaired neutrons occupies an$i_{13/2}$ orbital while the second one settles in a negative parity orbital, i.e. the configuration is$\pi 1h_{9/2}\otimes\nu 1i_{13/2}\nu j$ with $j = (3p_{1/2}, 2f_{5/2})$. Thus the positive parity of the band is caused by the involvement of the negative parity low j orbital.

In ^{192}Tl such a band will involve three odd neutrons (two $i_{13/2}$ neutrons and one low j negative parity neutron) coupled to the odd proton, with configuration $\pi 1h_{9/2}\otimes\nu 1{i_{13/2}}^2\,\nu j$. In order to study further such an option one has to determine unambiguously the spins and parities of bands 2 and 3, which is being planned.

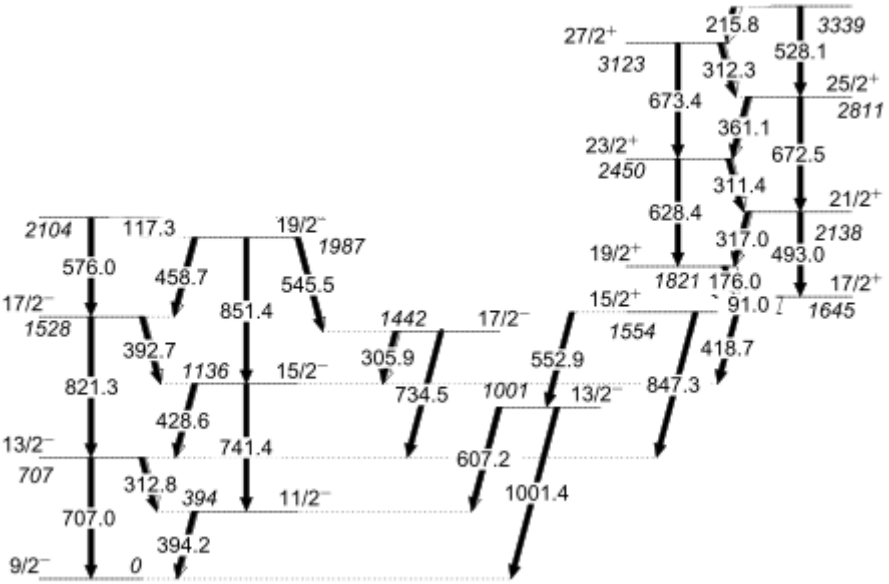

Fig 4-50 ^{195}Tl even parity band

5. Conclusion

This work had more than one objective.

One of the main objectives of this work was to learn and understand how to perform gamma spectroscopy research, starting from the beginning of an experiment until the final presentation of the data and interpretation of the results. This covered learning how to choose fusion evaporation reaction in order to produce the nucleus of interest ^{192}Tl, and the role the beam energy plays. It included hands on experience with setting up the experiment, such as adjusting pole zero and CFD thresholds and also an understanding of the basics of the electronics needed to operate the AFRODITE array. Furthermore the principles of the detection of gamma rays, the basic characteristics of gamma ray detectors, their properties and operation were studied. The data would be impossible to analyse without the preliminary data manipulations, such as gain matching, energy calibrations, Doppler shift corrections, as well as the gain drifts corrections which proved to be a formidable task. Sorting the data and constructing $E_\gamma - E_\gamma$ matrices completed this preliminary analysis.

Another objective was to extend the previously known level scheme. More than 50 new transitions were placed in the level scheme forming three new bands. Understanding how

rotational bands are formed (in the framework of the PRM) was the next step. A crucial role is often played by the Coriolis force which breaks pairs and aligns the odd neutrons along the rotational axis. Furthermore the method of comparing with the rotational bands in the neighbouring isotones and isotopes in order to explain the observations proved invaluable.

Another task that was set was to investigate the possibility of a chiral partner to the yrast band. But unfortunately such band was not found in our data. It is my opinion that a chiral band exists for ^{192}Tl based on trends in the neighbouring nuclei. Further studies with increased statistics in ^{192}Tl might reveal such bands. We can also have another look at our data after adding to it the data set collected with the thick target.

The study of the^{192}Tl thin target is in no way complete yet, since spin and parity measurements, etc. are not performed. A future study will focus on these and other quantities.

6 References

[Bru11] Jorg Brutcher Influence of P/Z setting on peak and lower spectrum cut off with MCA16, 18 December 2011,< http://www.gbs-

elektronik.de/fileadmin/download/manuals/mca_pole-zero-adjustment.pdf>

[Cae11] CAEN digital pulse height analyser-a digital approach to radiation spectroscopy (2011), accessed 18 December 2011,
<http://www.caen.it/documents/News/32/AN2508_Digital_Pulse_Height_Analyser.pdf>

[Dra96], N. Drakos (1996), Studies of excited nuclear states by using the gamma-gamma coincidence technique, accessed,18December 2011,

<http://www.nuclear.kth.se/courses/lab/latex/gammagamma/gammagamma.html>

[Ele06] Electronics for physics experiments lecture notes, department of physics, university of the Western Cape

[Exo11] EXOGAM detectors, accessed 18 December 2011,

<http://pro.ganil-spiral2.eu/laboratory/detectors/exogam/exogam-detectorstern Cape, 2006, page 30 and 40 fig 70

[Fer06] K. Ferlic, The phenomenon of pair production (2006), accessed 18 December 2011,< http://ryuc.info/creativityphysics/energy/pair_production.htm>

[Fra97] S. Frauendorf, J. Meng, Nuclear Physics A 617 (1997) 131

[Gam11] Gamma spectrum Generator, accessed 18 December 2011,
<http://www.nucleonica.net/wiki/index.php/Help:Gamma_Spectrum_Generator>

[Haw98] D. Hawcoft, Zakpopane school of physics 1998, Search for hyperdeformation in Uranium isotopes < http://ns.ph.liv.ac.uk/posters/dh/poster.html#introduction>

[Kra88] Kenneth S. Krane, Introductory nuclear physics, by John Wiley & Sons, Inc. Page 213-217, 198-204, 416-419.

[Kol11] D. Kollar, Pulse processing and analyses, accessed 18 December 2011,

< http://www.dnp.fmph.uniba.sk/~kollar/je_w/el3.htm#6> 213-217

[Kre79]A. J. Kreiner, Physics Review C, 21, (1980),page 937, High-spin band structure on 192Tl

[Law11] Elena Lawrie, iThemba Labs, Nuclear structure lecture notes (2011), Page 8, 12, 19 and 51

[Lab11] Attenuation of photons, national physics laboratory (2011), accessed 18 December 2011, <http://www.kayelaby.npl.co.uk/atomic_and_nuclear_physics/4_2/4_2_2.html,>

[Nil12] Nilsson diagram, accessed 5 January 2012 <http://www.wiley.com/legacy/products/subject/physics/toi/toi.pdf>

[Nuc12] Compton continuum, nucleonioc net, accessed 5 January 2012 <http://www.nucleonica.net/wiki/index.php?title=File%3ADetector_Response_Components_Spectrum.jpg>

[Mid11] MIDAS data acquisition system, accessed 5 January 2012,

<https://daq.tlabs.ac.za/>

[Obe11] Obed Shirinda and Elena Lawrie, iThemba Labs, Chiral symmetry in real nuclei (2011), lecture slides

[Pra10] D.A.E Symp.on Nucl. Phys. 55 (2010),P.N. Prashanth, Clover detectors set-up for the study of beta decay spectroscopy,

[Rad00] Online information on Radware (2000), accessed 18 December2011

<http://radware.phy.ornl.gov/info.html>

[Ran06] Ranjan Bohwmik, Inter university accelerator centre, New Delhi, Experiments with large gamma detector arrays lecture slides 4 (2006)

[Rud10] Rudolph Nchodu, Department of Physics, University of the Western Cape, 2010, lecture notes,

[Sha10] John F. Sharpey –Schafer, Department of physics, university of the Western Cape lecture notes (2011) page 87

[She98] Sara Shepherd Segmented germanium detectors (1998), accessed, 18 December 2011< http://ns.ph.liv.ac.uk/posters/sls/poster.html>

<http://radware.phy.ornl.gov/info.html>

[Wan10]ShuangQuan B. Qi, S.Y. Wang, Zhang School of Physics, Peking University lecture slides (2010), Static chirality and chiral vibrations of atomic nuclei in particle rotor model,